# A review of microstructured optical fibers for sensing applications

Pingsheng Xue[1,2], Qiang Liu[1,2,3*], Shuncheng Lu[2], Yongwei Xia[2], Qiang Wu[4], and Yongqing Fu[4]

1. *College of Information Science and Engineering, Northeastern University, Shenyang 110819, China*
2. *School of Control Engineering, Northeastern University at Qinhuangdao, Qinhuangdao 066004, China*
3. *Hebei Key Laboratory of Micro-Nano Precision Optical Sensing and Measurement Technology, Qinhuangdao 066004, China*
4. *Faculty of Engineering and Environment, Northumbria University, Newcastle upon Tyne NE1 8ST, U.K.*

*Corresponding author.

E-mail address: liuqiang@neuq.edu.cn (Q. Liu).

**Keywords :** microstructured optical fiber; fiber sensor; fiber fabrication; sensing application

---

**Abstract**

Microstructured optical fibers, including not only photonic crystal fibers but also new types of fiber with different configurations on the cross section, are elaborately designed and they usually have special application purposes among which sensing is one of the most common. In this review we first summarize fabrication methods and transmission mechanisms of microstructured fibers. And then application examples using fibers with special and novel microstructures in strain/pressure/bending/twist, temperature, flow rate, electric/magnetic field, humidity, gas, refractive index and chemical/biochemical analyte sensing based on various principles are introduced. Finally, state of the art and developing trends as well as challenges faced by sensing technology based on microstructured optical fibers were discussed.

## 1. Introduction

Microstructured Optical Fibers (MOFs), as a transmission medium of lightwaves, due to their excellent characteristics such as flexibility in structural design, resistance

to electromagnetic radiation interference, corrosion resistance, high temperature resistance and low transmission loss, have been widely used in communications, biomedicine [1], engineering [2], optical sensing [3] and many other fields. With the continuous improvement of MOFs manufacturing process and the pioneering functional designs, now based on MOFs, high-power fiber lasers [4], wide-bandwidth polarization splitters [5], supercontinuum sources [6], fiber couplers [7], microfluidics devices [8], high-sensitivity fiber sensors and many other micro-nano photonic devices with excellent performance have been developed.

Mentioning microstructured fiber, people usually come across the photonic crystal fiber (PCF) [9]. However, the generalized microstructured fiber also includes not only PCFs but various new type fibers with different structures in the fiber cross section, such negative curvature anti-resonant fiber (ARF) [10], side hole optical fiber [11], suspended core optical fiber [12] and hollow core optical fiber [70] etc., they have different characteristics like tunable dispersion [13], high nonlinear [14], low transmission loss [15], tunable transmission windows [16], enhanced evanescent field [17], and high birefringence [18] etc. In last 20 years, researchers have proposed numerous fiber optic sensor structures based on various principles for different measurement and application needs. By now, some types of fiber optic sensors like temperature, displacement sensors and gyroscope have already been utilized in practice [19-21]. However, sensors based on traditional optical fibers may no longer meet some special measurement requirements in reality because of low sensitivities (like fiber grating, though the temperature response is linear and wide-range, the sensitivity is low) and structure limits (light are confined inside the fibers and difficult to interact with the environment). Since the first PCF was produced in 1996, new fibers with novel microstructures have been designed and fabricated continuously, which provide a better platform for researchers to develop new type fiber-optic sensors. The advantage of MOFs is that the structure can be better designed for the needs of sensing object and to achieve optimal performance by enhancing the influence of factors on lightwaves. Due to the diversity structures of MOFs and their excellent optical properties, researchers in recent years have favored the use of MOFs to develop new optical fiber sensors based on different sensing mechanisms. At present, the sensing mechanisms of fiber sensors

mainly include grating [22], interferometer [23,24], surface plasmon resonance (SPR) [25] and absorption [26] etc. Sensors based on MOFs have been used in the measurement of many parameters such as refractive index (RI) [27], temperature [28], stress [29], as well as chemical and biomedical detections [30-32]. Optical fiber sensing technology based on the MOFs has aroused extensive research interest especially infiltrating the MOFs with functional materials and further set off a wave of researches on Lab-in-Fiber technology [33,34], which greatly expands the application range of optical fiber sensors.

In this review, we discuss various structures of MOF and focus on their sensing applications in different fields. Fig. 1 shows the arrangement of whole article. We first go through the current fabrication methods of MOFs briefly, then we classify the fibers, summarize the transmission mechanisms in MOFs with different structures and how theses fibers may be utilized in sensing. Followed by exampling several sensing applications of MOFs with interesting novel structures in different sensing fields including measurements of strain, temperature, electric/magnetic field, gas, chemical and so on. And finally we conclude with discussion on the developing trends of MOF sensors and the prospect of the MOFs.

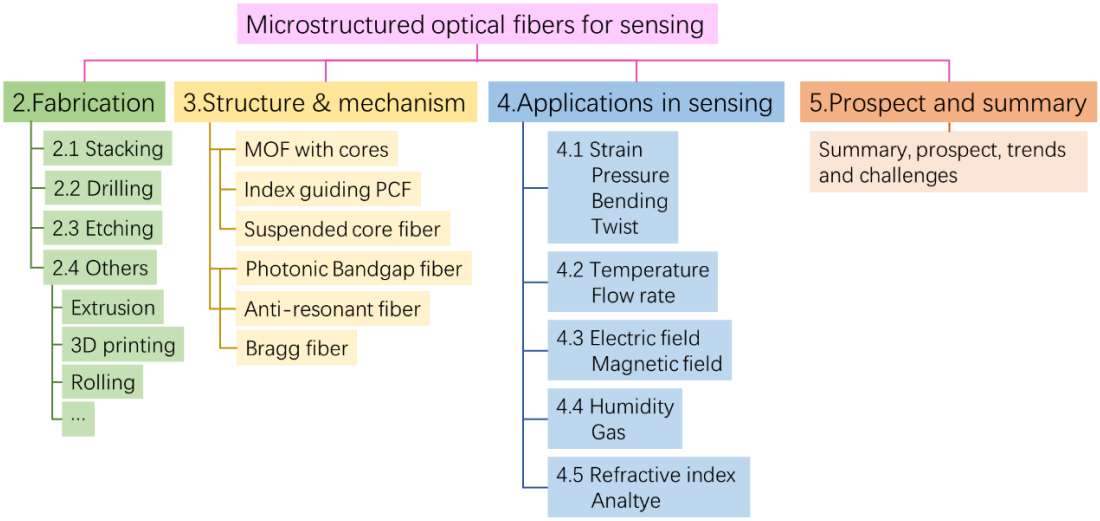


**Fig. 1** Structure schematic of the review.

## 2. Fabrication

At present, optical fibers are drawn from preforms on a fiber drawing tower. Preform is sent by feeding mechanism at the top of the tower into furnace to be softened and then drawn into thin fiber by contact rollers. The preform structure defines the cross

section of fiber, so the preparation of preforms are vital for fabrication of MOFs, here we list the methods of making MOF preforms.

*2.1 Stacking*

Stack and draw method [35] is a conventional way to fabricate PCF or other microstructured fiber with period air holes. Fiber preforms are made with capillaries or rods stacking in a larger tube. The cross section of fiber, air hole distribution, air hole sizes and pitches can be flexibly adjusted by the dimensions of the capillaries and rods and stacking arrangement. During thermal drawing on the fiber drawing tower, usually nitrogen, argon or other protective gases are ventilated into the preform with precisely controlled pressure to maintain the air holes not collapsed and adjust the hole sizes, which is the main difficulty in fabricating these fibers. Sometimes two or more drawing steps are needed to achieve ultra-tiny air hole structures like super-lattice PCF [37]: firstly, draw the stacked capillaries into canes in millimeters diameters, then stack again the canes into the second preform and draw again to final fibers. PCFs designed for sensing have various structures [36]. The advantage of stack and draw method is the flexibility to adjust the designed structure, not only PCF, this method is also competent for all-solid fibers such as multi-core fibers, and by using proper size capillaries and controlling pressure, suspended core fiber can also be fabricated with this method [56].

*2.2 Drilling*

Drilling holes on a thick glass rod is another way to fabricate preforms of the MOF [38]. Suspended core fibers and side hole fibers are usually fabricated by this method [39,40]. However the ordinary drill is not suitable for glass materials, the impact and heat during drilling will easily crack the preform. Usually ultrasound drilling machines are utilized to make holes on glass fiber preforms [41]. Holes are grinded by abrasive which is mixed with water and driven by ultrasound high-frequency vibration, the suspension will cool down the drilling surface and prevent the glass from cracking. Ultrasound drilling is extremely suitable for hard and brittle materials such as optical glass and ceramics, but limited by the length of drilling tools the drilled hole depths are usually less than a dozen centimeters. The holes will form air channels in fiber after drawing, or, high index rods and stress parts can be insert into the drilled holes in the preform to produce multi-core, eccentric core or high birefringence fiber. Compared

with stack and draw, the fiber structure during drawing is more stable with drilling hole method. The main disadvantage of ultrasound drilling is time consuming, so this method only suits for fibers with simple structures.

*2.3 Etching*

Etching method [42] is suitable for materials which do not react with acids. The fiber preform is stacked with two different types of glass rod or capillary: one can be dissolved by acid while the other cannot. After heating to adhere and fuse each rod or capillary, the part which can be etched is removed by submerging the preform into acid. Die-cast process [43] is in the same way of etching method, but suitable for low softening temperature glass, whose softening temperatures are lower than metal. Softened glass is pressurized into the pre-designed metal mold, after slowly annealed to room temperature, similar to the etching method, the metal parts are removed by sulphuric acid, leaving air channels in the glass preform.

*2.4 Others*

Many other methods to fabricate MOF were also proposed by researchers. Extrusion is another way to fabricate preforms made of low softening temperature glass [44]. The balk glass is heated and extruded by air pressure into the specific structure mold, forming preforms with air channels. Preforms with channels may also be produced with a mold by sol-gel method. Lasers have high power and able to etch glass, [45] etched air channels on a silica column with a switching-Q laser and finally fabricated PCF. In [46-48] 3D printing technique was applied to make polymer MOF preforms. With 3D printing technique, it has become very convenient to obtain polymer fiber preform with special structures which can be designed in software. Silica preform 3D printing is also becoming accessible [49]. Multi-layer and multi-material polymer performs can be made by rolling thin polymer films around a rod and then consolidating, which is an already mature technique [126]. A microstructure polymer fiber direct fabricating device was designed in [50], enables drawing polymer fibers directly on table instead of thermal drawing on the tower.

Fig. 2 shows the schematic of the MOF fabrication methods. Methods for producing microstructure fibers are still developing, towards the goal of stable, efficient and low-costing.

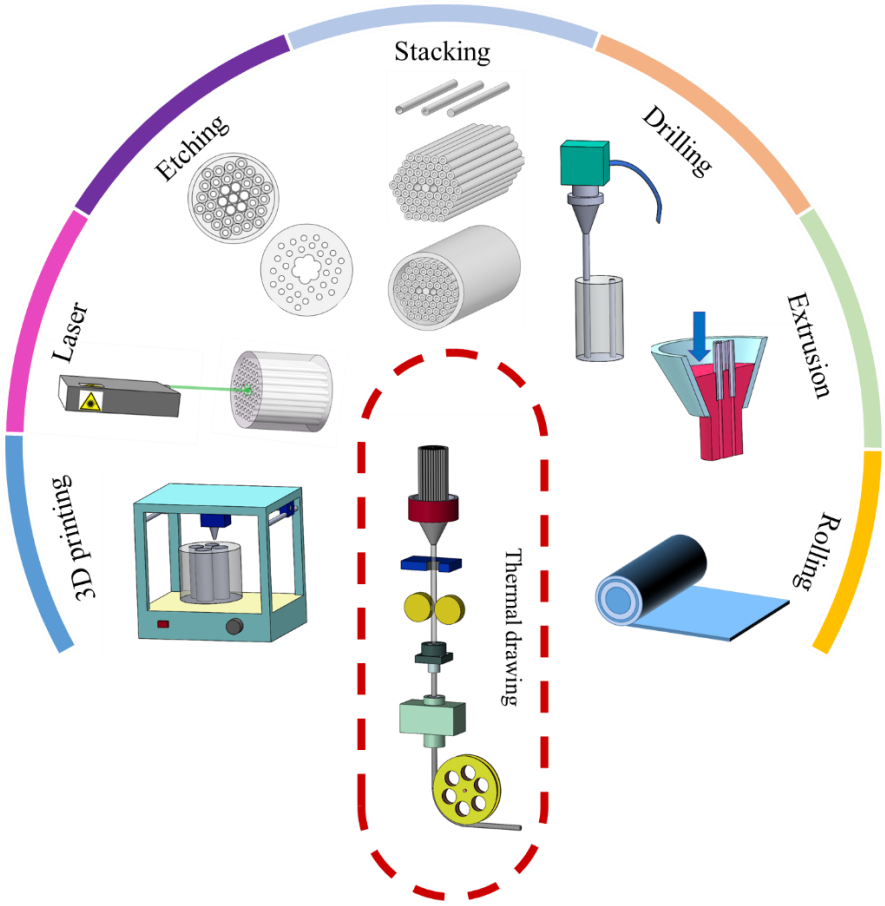


**Fig. 2** Fabrication methods of the MOFs.

## 3. Structure & mechanism

The guiding mechanisms of MOFs are different and related to fiber structures. For the fibers with cores whose indices are slightly higher than the background silica (Fig. 3(a)), there is no doubt that the light will transmit in the cores, which is the same principle with conventional fibers like single-mode fiber (SMF) and multi-mode fiber (MMF). The cores may not locate in the center, microstructures like hollow channels in these MOFs will satisfy the required detection conditions and improve the sensing performance by lightwave coupling or forming interferometer, specific examples can be found in Section 4. However, for the fibers made of pure materials which do not have higher index cores, light can be guided either in the background materials or in air, depend on the fiber structures. The light transmission follows total internal reflection (TIR) mechanism in the index guiding PCF (Fig. 3(b)) and grapefruit-like suspended core fiber (Fig. 3(c)), which is similar to the common step-index fiber. In the index guiding PCF, light is confined in the center which is surrounded by periodically arranged air holes. Size and distribution of the air holes may bring the fiber with

characteristics like adjusted dispersion, high-nonlinear or high birefringence. The high birefringence PCF is widely used in fiber gyro [20] for its polarization-maintaining characteristic as well as in strain/pressure sensors, in which the sensing factor causes changes in birefringence. The holes in cladding are also good platforms for infiltrating sensitive liquids whose RI are usually lower than silica so that TIR transmission mechanism is maintained, RI of liquid in cladding will modulate the fiber mode effective indices causing the transmission properties varying with sensing factors. The grapefruit-like suspended core fibers, in which the core is not covered by silica cladding, can not only modulate the mode effective indices but also increase the amount of light power in the surrounding, enhancing interaction between light and filling fluid, moreover, the suspended core can be made very thin, with a diameter close to wavelength it can work as a micro/nano fiber while the outer silica serves as a protection layer, it is more robust and reliable than the exposed conventional micro/nano fibers in sensing applications.

While the light can transmit in the air in fibers like hollow-core PCF (Fig. 3(d)) and ARF (Fig. 3(e)) [52,53]. Because the light transmits in the hollow core, these fibers are well applied in gas sensing, realizing total light-gas overlap and maximizing absorption efficiency. In the hollow-core PCF, which is also known as photonic bandgap (PBG) fibers, the guidance follows PBG mechanism [51]. The PBG cladding is two-dimensional quasi-photonic crystal structure consisting of silica and air channels which are strictly arranged in size, pitch and period, when light incidents on the interface of the hollow core and cladding air holes, only light of specific wavelengths and certain angles of incidence are directed back to the hollow core and propagate forward along the fiber, forming a bandgap on spectrum. In the ARFs, light propagates in the low index center (usually air) which is surrounded by high index layers/tubes. In transverse, the high index layers/tubes can be considered as Fabry–Perot (F-P)- like resonators. Wavelengths that meet F-P conditions corresponds to the transmission minima in spectrum, which can be calculated by: $\lambda_m = 2(d\sqrt{{n_1}^2 - {n_2}^2})/m$ ($n_1$: high index, $n_2$: low index, $d$: thickness of high index layer, $m$: integer), while the anti-resonant wavelengths can transmit in the low index core which corresponds to the high transmission. The transmission windows are wide and can be adjusted by controlling

the thickness of resonate layers, which are advantages in gas and chemical sensing. In the fiber that consists of a low-index core surrounded by multiple high and low index layers (usually called Bragg fibers) (Fig. 3(f)), Λ is the lattice pitch. Note that for shorter wavelengths, approximately when λ<Λ, transmission follows anti-resonant reflecting optical waveguide (ARROW) model, the transmission minimum wavelengths are mainly decided by the thickness of high index layers. For longer wavelengths, λ>Λ, the multiple layers of the cladding form 1D photonic structure and the transmission can be considered following PBG mechanism, transmission properties are mainly consisted with the lattice period [54].

Fig. 4 exhibits some fibers with novel structures designed for sensing in recent years. Suspended multi-core fiber Fig. 4 (a) can be used in curvature sensing because of its asymmetry; fibers in Fig. 4 (b)(d)(f) enabled large overlap between light and liquid or gas; fibers in Fig. 4 (c)(e)(g) are highly birefringent and suitable for strain and pressure sensing. Sensing application of MOFs like these will be discussed in next section.

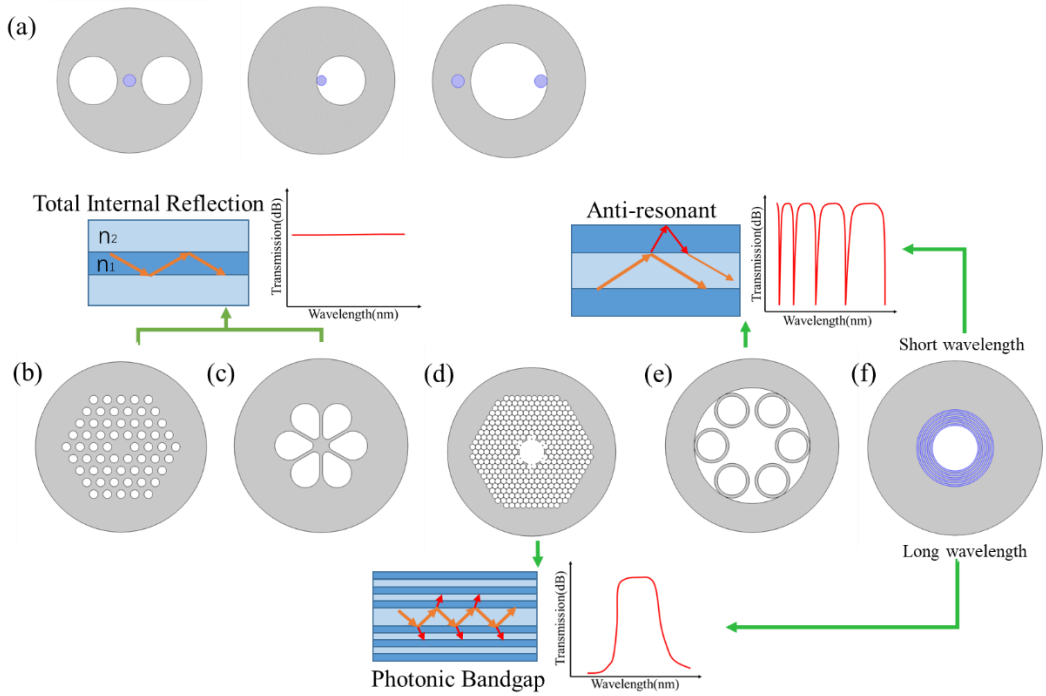


**Fig. 3** (a) MOF with cores and channels, light transmit in cores like common fiber. (b) Index guiding PCF and (b) Suspended core fiber, follows total internal reflection. (c) Photonic bandgap fiber (hollow core PCF). (d) Anti-resonant fiber. (e) Bragg fiber, follows anti-resonant guidance at

short wavelength and photonic bandgap guidance at long wavelength. (blue in the schematics represents high index rods or layers, $n_1>n_2$).

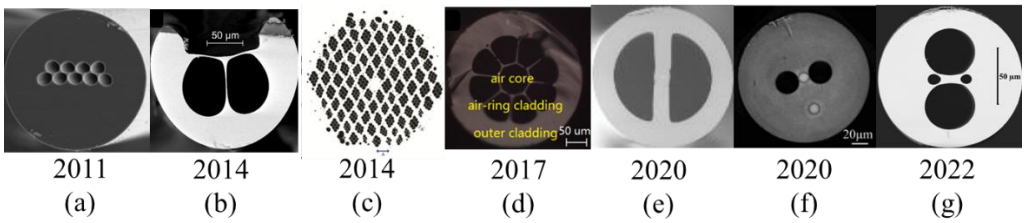


**Fig. 4** (a) Suspended multi-core fiber [132]. (b) Exposed core fiber [27]. (c) Super-lattice PCF [37]. (d) Anti-resonant fiber [70]. (e) Two semicircular-hole fiber [133]. (f) Twin-core dual-hole fiber [41]. (g) Four-hole asymmetric-shaped fiber [137].

## 4. Applications in sensing

In this section, we give examples of MOFs in sensing. Fig. 5 shows the application fields of MOF sensors. The researches on MOF sensors are countless, here we focus on introducing fibers with special structures which were elaborately designed, novel or based on which have better performance in sensing applications, most of them are self-made by the researchers and may not commercially available. We will discuss these examples classified by sensing fields like strain/pressure/bending/twist, temperature, electric/magnetic field, humidity, gas and so on. Various principles are well covered by examples we selected in this section.

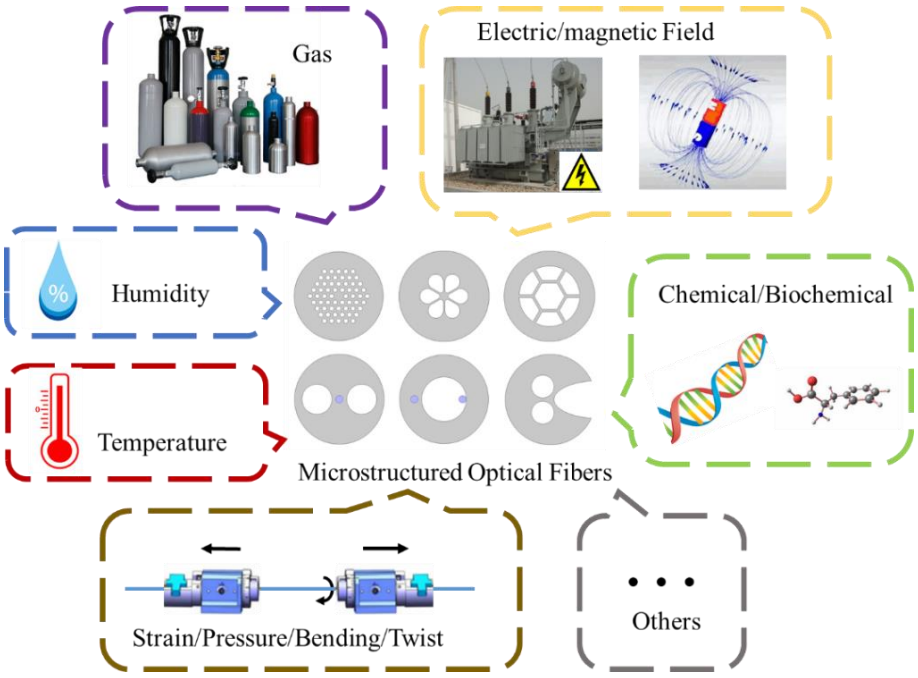


**Fig. 5** Sensing application fields of the MOF.

### *4.1 Strain/pressure/bending/twist*

The most basic application of the MOF is force or mechanical deformation sensing

such as strain [55-57], pressure [60,61], bending [58,59] or twist [56,62,63]. These sensing are extremely important in industrial, aerospace, civil engineering, military, marine and atmospheric sciences. In working scenarios, force or deformation directly affects transmission properties of the MOFs. Compared with all-solid conventional fibers, the influence of strain, stress or pressure can be magnified in MOFs, for example, because of the air holes in cladding, PCFs are more elastic than standard fibers, which means higher sensitivity in strain or stress sensing.

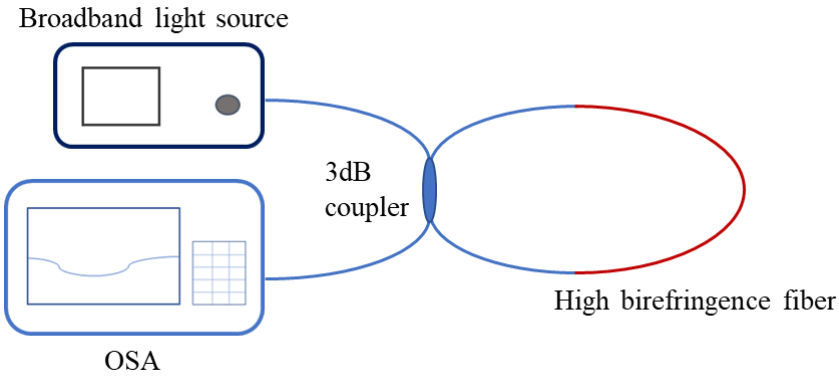


**Fig. 6** Schematic of the Sagnac interferometer embeded with high birefringence fiber.

Sagnac interferometers embedded with high birefringence fibers (Fig. 6) are widely investigated [24,55,56,63] in strain, stress or pressure sensing. In these Sagnac interferometers, light from board band source incidents into the input of 3 dB coupler and circle both clockwise and counter-clockwise in the fiber loop embedded with a section of high birefringence fiber. The effective index for two orthogonal modes $n_{eff}^{x}$ and $n_{eff}^{y}$ in high birefringence fiber are different. Phase difference induces between x and y polarization direction of two opposite circling beams. Interference dips can be observed with an optical spectrum analyzer (OSA). The transmission of Sagnac interferometer is:

$$T = [1 - \cos(2\pi BL/\lambda)]/2 \quad (1)$$

In which, $B = |n_{eff}^{x} - n_{eff}^{y}|$ is the birefringence, $L$ is the length of the high birefringence fiber. Interference dips show up on spectrum when $2\pi BL/\lambda = (2m + 1)\pi$, $m$ is an integer. Strain, stress or pressure which cause change in the birefringence $B$ will result in the shift of the interference dips. Sagnac interferometers take advantage of the birefringence of MOFs and usually have high sensitivity in strain and pressure sensing. In [56] a high birefringence suspended core fiber (HB-SCF) fabricated by

staking two different sizes of capillaries to form an elliptical core in the center (Fig. 7(a)) is investigated for multiple sensing applications. By forming the fiber into Sagnac interferometer (Fig.7 (b)), spectrum can respond to strain, hydrostatic pressure and torsion. The strain and hydrostatic pressure sensing can be realized by directly observing the shift of interference dips (Fig. 7(c)), the torsion sensing, which depends on the variation of dips extinction ratio, it is more intuitive by observing the amplitude of the peak in fast Fourier transform of the interference spectrum. Because of its suspended elliptical core, the birefringence changes induced by pressure is larger than all-solid fiber and shows better sensing performance than normal polarization fiber (PMF), the sensitivities are 0.43pm/με for strain, 2.82nm/MPa for pressure and 0.0157/° for torsion. Cascaded Sagnac loops can further enlarge the sensitivity by vernier effect, a sensitivity as high as 45.15 pm/με for strain sensing is achieved with two polarization maintaining PCF (PMPCF) loops in [55]. Normally, PMPCF can have high birefringence by inducing different sizes of air holes. Other than that, elliptical air hole PCF is also highly birefringent, but it is extremely difficult to be fabricated, an alternative approach is super-lattice PCF, which replaces the air hole with elliptically shaped super-lattice structures, can be fabricated by two-step drawing. A pressure sensitivity of 1.6 nm/MPa is obtained with super-lattice PCF in [37].

The high birefringence MOFs exhibits multiple uses in physical parameters sensing and they are reliable. Compared with panda PMF which has stress bar in cladding and easily influenced by temperature fluctuation, the high birefringence MOFs shows less cross sensitivity. Other sensing principles besides Sagnac include grating and Mach–Zehnder interferometer (MZI) [57], they take advantage of the more elastic features of MOFs than solid fibers, due to the porous structure.

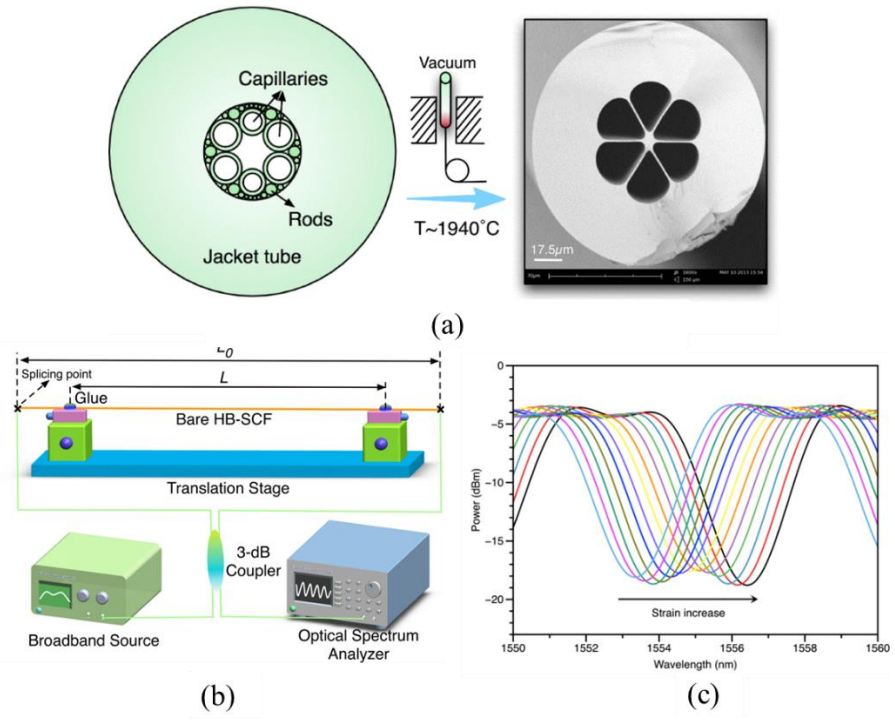


**Fig. 7** (a) Schematic of the fiber preform stacking and fiber cross section in [56]. (b) Strain measurement constructed with the fiber. (c) Spectrum of the Sagnac interferometer as strain increasing.

Bending or curvature is another type of deformation which also can be measured by MOFs (Fig. 8(a)). G. Mao et al. designed a hollow twin core fiber (Fig. 8(b) inset) [58]. The cores are embedded in the wall of the capillary, FBGs were inscribed on both cores. When the fiber bends in the direction of the connection line of two cores, the FBG on upper core is compressed while the lower is stretched, the FBG wavelengths of two cores shift in opposite direction (Fig. 8(b)), in which way the sensitivity is doubled by measuring the difference between FBG wavelengths, while the temperature influence is compensated by the same shift direction of the two dips. The asymmetry of MOFs is also a merit in discriminating bending direction compared with conventional fibers, by demodulating intensities of each core of an asymmetric air-hole multicore fiber, bending vector sensor is achieved in [59].

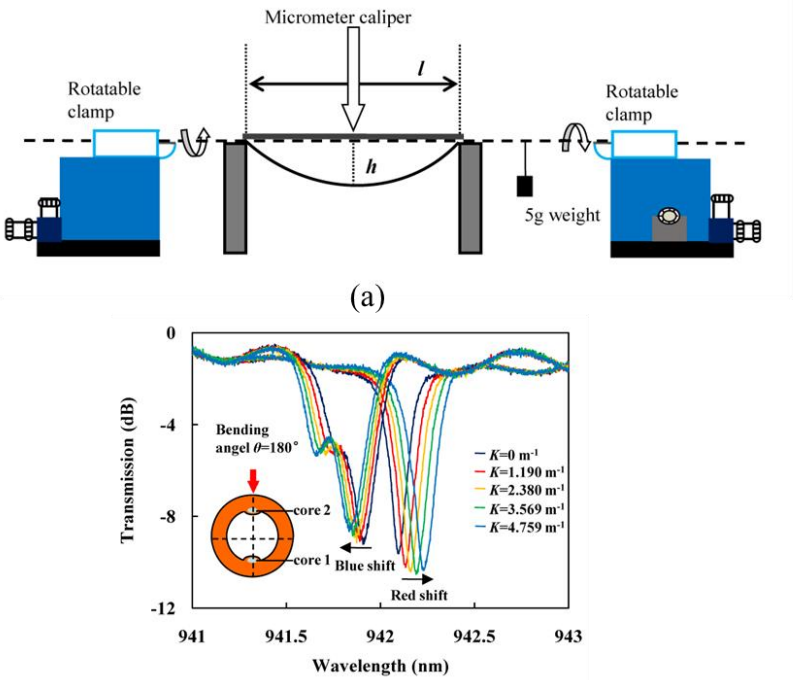


**Fig. 8** (a) Bending sensing setup in [58]. (b) The measured transmission spectra for different curvatures. (Inset: Structure of the hollow eccentric twin core fiber.)

Helical microstructured fiber [64,65], which is competent for twist sensing, usually can directly discriminate the twist direction. In [65], W. Shin et al. fabricated a PCF based helical long-period fiber grating (HLPG) (Fig. 9(a)) by $CO_2$ laser heating, core mode couples to cladding mode as a result of helical period structure. The resonant wavelengths of the long period granting is given by:

$$\lambda_i = (n_{core} - n^i_{cladding})\Lambda_g \tag{2}$$

in which $n^i_{cladding}$ is the *i*th cladding mode, $\Lambda_g$ is the period of grating. One twist direction will enlarge the helical grating period while the other does the opposite, causing the resonant dips red or blue shift (Fig. 9(b)). High birefringence MOFs are also able to be used in twist sensing based on their polarization maintaining characteristic [56], but the twist angle are usually limited in 90˚.

Table I summarized the representative strain, bending, pressure or twist sensors based on MOFs.

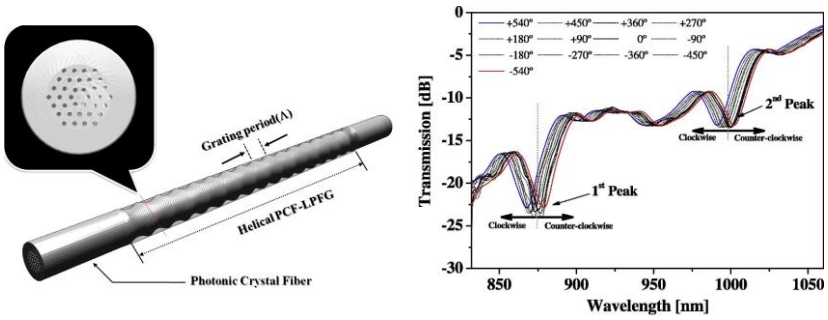


(a) (b)

**Fig. 9** (a) Helical PCF long-period grating in [65]. (b) Spectral response of the helical PCF versus rotation angle.

**Table. I Sumary of MOF Strain/pressure/bending/twist sensor**

| Ref. | Factor | Fiber | Principle | Performance |
|---|---|---|---|---|
| [55] | Strain | PMPCF | Sagnac | 45.15 pm/με |
| [57] | Strain | Twin-core PCF | Mach–Zehnder | -0.31 pm/με |
| [37] | Pressure | Super-lattice PCF | Sagnac | 1.6 nm/MPa |
| [60] | Pressure | Side-hole fiber | Rocking filter | 132 nm/MPa |
| [61] | Pressure | Embedded-core capillary fiber | Lyot filter | 1.04 nm/bar |
| [58] | Bending | Hollow twin core fiber | Grating | 33 pm/$m^{-1}$ |
| [59] | Bending | Asymmetric air-hole multicore Fiber | Intensity variation | -- |
| [132] | Bending | Suspended multi-core fiber | Mach–Zehnder | -4.34 dB·m |
| [62] | Twist | Suspended twin-core fiber | Sagnac | $1.2\times10^{-2}$dB/° |
| [63] | Twist | Side-Leakage PCF | Sagnac | 0.9354 nm/° |
| [65] | Twist | Helical PCF | Grating | -17.45 pm/° |
| [133] | Strain<br>Twist | Two semicircular-hole fiber | Mach-Zehnder | -1.32 pm/με<br>5.01 nm/° |

*4.2 Temperature, flow rate*

Temperature sensing is common in all application fields. But because the thermo-optic coefficient of silica is limited, to improve the temperature sensing ability, materials with high thermal expansion or thermal-optic coefficient are integrated in the fiber, MOFs with air holes are good platforms for carrying these materials [66-69].

An ultrahigh-sensitivity temperature sensor based on resonance coupling in a side-

hole fiber infiltrated with thermal adjustable RI liquid (Fig. 10(a)) was proposed in [68]. The holes were about 20 μm and infiltrated liquid for about 1 cm. Resonant dips appear at which wavelengths the $LP_{01}$ core mode and liquid rod modes meet the phase matching condition (Fig. 10(b)(c)):

$$n_{eff}^{core}(\lambda(T),T) = n_{eff}^{rod}(\lambda(T),T) \tag{3}$$

When temperature rises, the RI of liquid decreases accordingly, induces the blue shift of the resonant dips. From 80-100˚C the sensitivity reaches 13.1 nm/˚C, which is relative high among the fiber temperature sensors. Waveguide coupling usually have high RI tuning efficiency [73,102], while holes of the MOFs near to the core provide conditions for the coupling between liquid rod modes and core modes. In coupling principle, the RI of liquids are usually higher than the fiber core, so the high order liquid modes whose effective indices is close to the core mode but with high loss can meet the phase matching condition. If the RI of liquids are lower than the fiber, instead of coupling they usually tune effective indices of the MOF transmission modes, based on which principle interferometers are more often designed [66]. Temperature ranges widely among various application scenarios like normal room, human body, seawater or even furnace and freezer. By infiltrating proper materials in MOFs, different measurement ranges can be satisfied [69], for example, since the boiling point of alcohol is 78.37 ˚C, temperature below 70 ˚C can be measured, other materials like ethylene glycol are suitable for higher temperature. However, liquid infiltrated fiber usually have difficulties when splicing with other fibers. Evaporation during splicing may blow up the hole and cause high insertion loss, meanwhile the fluidity also impairs the stability of sensor.

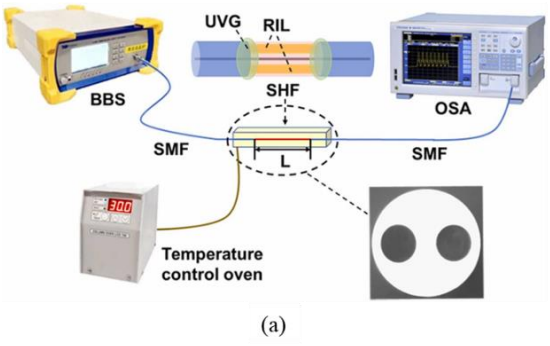


(a)

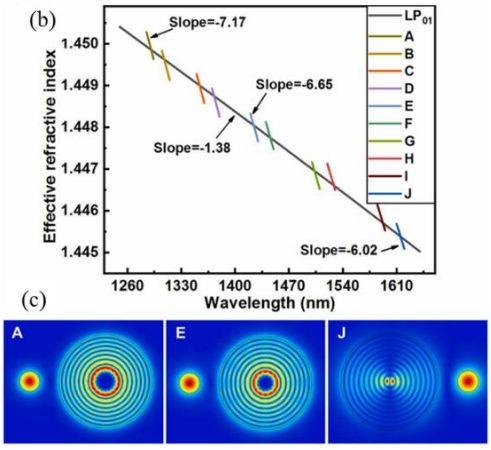

**Fig. 10** (a) Temperature sensing setup with the side-hole fiber (inset) in [68]. (b) Mode dispersion curves and (c) Mode field profiles of the coupling between liquid mode and core mode in the fiber.

Solid materials which can be melted are also able to be infiltrated in MOFs to realize temperature sensing. In [67], a side-hole PCF filled with metal (Fig. 11(b)(c)) was fabricated and embeded in a Sagnac interferometer, the thermal expansion of metal in the outer cladding brings changes in birefrigence due to stress (Fig. 11(d)(e)), resulting interference dips shift with varying temperature. Bismuth (Bi) and indium (In) were filled the side hole in outer cladding, they are solid state in the measuring ranges of 22.4°C–46 °C and 21.6°C–70.7°C, and the sensor have a sensitivity of -9.0 nm/°C highest. This work presents the potential use of a new type of fiber, and testifies an approach that the infiltrated material can be not only thermal-optical liquid but also high thermal expansion solid which could induce stress to the fiber core. The solid has no fluidity which benefits the stability of sensor. Table II lists MOF based temperature senors with their fiber type, infiltrared material and performaces. Without infiltrating sensitive materials, MOFs made of pure silica usually have lower temperature sensitivity than other fibers. For example, birefringence changes of the PMPCF caused by thermal is much lower than the Panda PMF, which means the pure silica MOFs have less influence of temperature when the fiber was used for measuring other parameters. While on the other hand, fibers can be made of materials sensitive to thermal themselves (such as polymer) so that no other infiltration procedures are needed to achieve both high sensitivity and convenience, as well as stability.

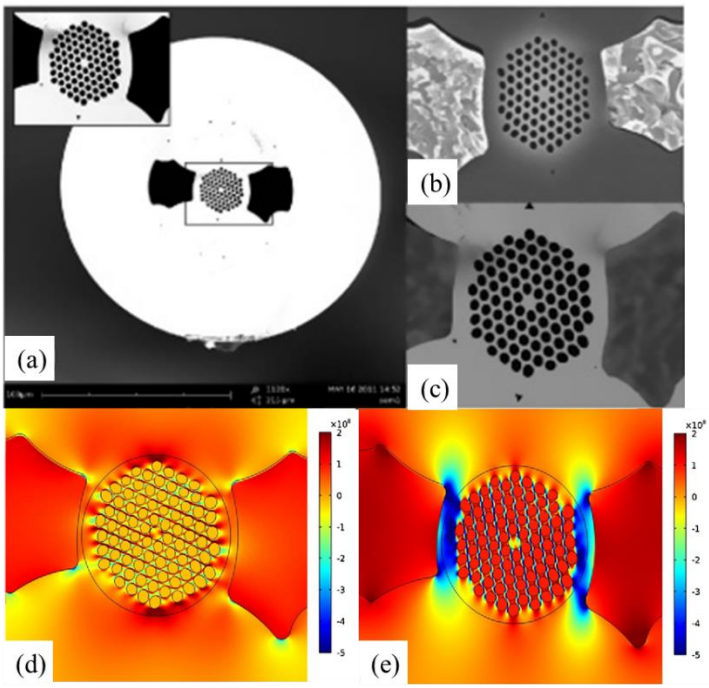


**Fig. 11** Images of the cross section of the side-hole PCF used in [67] with different filler metals:(a) unfilled, (b) Bi, and (c) In, (d) the stress tensor profile on x direction and (e) y direction at 45 ˚C.

**Table II. Summary of the MOF temperature sensor**

| Ref. | Fiber | Material | Principle | Performance |
|---|---|---|---|---|
| [66] | PMPCF | Glycerin | Sagnac | 1.5005 nm/ ˚C (25°C -85 °C) |
| [67] | side-hole PCF | Metal | Sagnac | -9.0 nm/°C (22.4°C–46 °C) |
| | | | | -1.80 nm/°C (21.6°C–70.7°C) |
| [68] | Side-hole fiber | RILs | Coupling | 13.1 nm/˚C (80°C -100°C) |
| [69] | Hollow core fiber | Alcohol | Anti-resonant | -0.48nm/ ˚C (--60 ˚C) |
| [133] | Exposed-core MOF | Liquid crystal | Mach–Zehnder | −558.5 nm/°C (31°C -32 °C)) |
| | | | | −6.7 nm/°C (34°C -110°C) |

Based on the temperature sensing principles, microfluidic flow rate sensors are also proposed by researchers (Fig. 12) [70]. With a heat source such as hot metal wire or laser continuously heating the fiber sensor, based on the thermal transfer, the microfluidic liquid flowing in the channel of MOF absorbs and takes away a part of the heat, microfluidic flow rate sensing can be then realized by monitoring the varying transmission properties caused by temperature change [71]. A flow meter based on graphene-coated microstructure hollow fiber was designed by R. Gao et al. [70]. Holes

were drilled on the side wall to let liquid in and out flowing through a channel in the fiber (Fig. 12(a) inset). Light follows anti-resonant guidance in the hollow core. The fiber was coated with a few layers of graphene (FLG) whose RI can be influenced by temperature and the reflection on the outer surrounding of anti-resonant wave guide changes. The light intensity corresponding to the resonant condition can be expressed as:

$$T_R = \frac{(1-rr')(r+r')}{1+r'^4-2r'^2} I_R \tag{4}$$

$T_R$ is the power of the resonant dip, $I_R$ is the input intensity $r$ and $r'$are reflection coefficients at air-silica and silica-FLG interfaces. With a constant powered laser heating the graphene-coated fiber (Fig. 12(b)(c)), the graphene coated layer temperature increases due to the optical absorption while the flowing liquid absorbs and takes away the heat, the reflection coefficients $r'$ changes with temperature which is consisted with flow rate, hence varies the light power reflected from the silica-FLG interface, flow rate can be obtained by measuring the intensity of the resonant lossy dip. Similarly, based on the thermal transfer, an anemometer which use alloy filled in MOF as hot wire and heated by a pump laser was designed in [129]. These flow meters based on thermal principle have pioneered new applications of the MOFs.

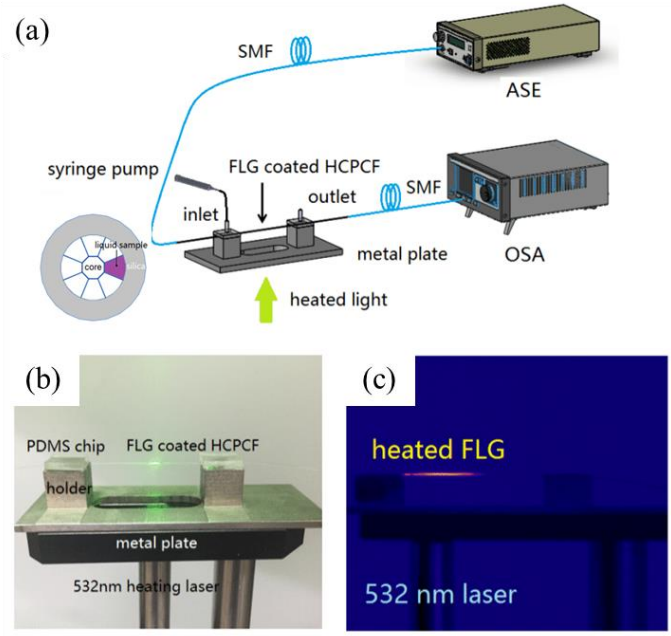


**Fig. 12** (a) Setup of the flow rate sensor designed in [70]. (b)(c) Heating the coated fiber with laser and measure flow rate based on heat transfer.

*4.3 Electric/magnetic field*

Immunity to electromagnetic interference is one of the best-known advantages of fiber sensor. However electric and magnetic field sensors which are vital in power industry need to be sensitive to the varying field. So in fiber electric field or magnetic field sensors, usually electro-optical or magneto-optical materials are induced to modulate the transmission properties of the fiber, which is similar to the temperature sensors discussed above. Liquid crystals (LC) and magnetic fluids are candidates for electric field [23,72,73] and magnetic field sensing [74-77], compared with other solid electro-optic and magneto-optic crystals which have to be in balks and resulting the sensor large in size, these liquids can be easily filled into the small air holes of microstructure fibers, realizing compact size of the sensor.

The rod-shape LC molecules will tilt to the electric field direction and the tilt angle increases with electric field strength so that the RI changes anisotropically and modulates fiber transmission properties. Besides sensors, devices like tunable polarizer [78], modulator [73] and optical switch can also be realized with LC infiltrated microstructured fibers. Y. Huang et al. [73] selectively infiltrated E7 LC in to one inner hole of a PCF (Fig. 13(a)). The selective infiltration of a single hole in MOF can be realized by femtosecond laser drilling over a specific air hole on a thin SMF cap spliced to the MOF. Since the innermost hole is filled with LC whose RI is higher than silica, the LC rod high-order mode couples with fiber core mode in phase matching condition. The LC infiltrated fiber is sandwiched between two electrode plates with applied voltage (Fig. 13(b)), and when LC is tuned by the parallel electric field intensity between electrode plate, the response of LC has a threshold of 60 V, above which the lossy dip starts shift sharply as voltage increases. (Fig. 13(c)). This LC selectively infiltrated PCF can be applied as an extremely high sensitivity electric field sensor, as well as wavelength-tunable electro-optical devices with very fast response, which is leading in performance. In [23], based on the asymmetric structure in fiber cross section brought by LC selective infiltration in PCF, electric field orientation is also considered.

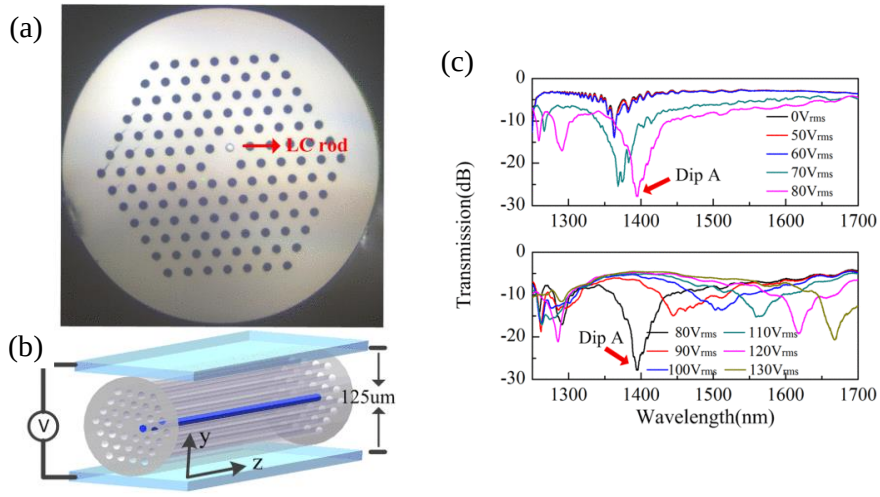


**Fig. 13** (a) Selective infiltrated LC in one hole of the PCF [73]. (b) Electric field electrodes was provided by electrodes. (c) Electric field sensing response.

Researches on MOF infiltrated with magnetic fluids for magnetic sensing were also widely carried out. An example which was proposed by J. Yin et al. (Fig. 14) used a double-clad microstructure fiber (DC-PCF in Fig. 12(a)) [76], in which center was a core of 8.93 μm. 24 micro channels divided the cladding into two parts. Nano-magnetic fluid was filled in the 24 micro channels by high pressure injection (Fig. 14(b)). By splicing with an offset between two fibers, light from SMF incidents into both the core and inner cladding of the DC-PCF and forms a MZI (Fig. 12(c)). The transmission of the MZI can be approximately expressed as:

$$I = I_{core} + \sum_i I_{clad}^{ith} + \sum_i 2\sqrt{I_{core} \cdot I_{clad}^{ith}} \cos(\varphi^i) \tag{5}$$

$$\varphi^i = 2\pi L(n_{eff}^{core} - n_{eff}^{clad,i})/\lambda \tag{6}$$

in which $I_{core}$ and $I_{clad}^{ith}$ are intensities of core and cladding modes, $\varphi^i$ represents the phase difference. Dip occurs when $\varphi^i = (2m+1)\pi$. $m$ is an integer. The magnetic fluid is isotropic when no external magnetic field is applied, as the magnetic field intensity increases, the particles in fluid agglomerate to chains along field orientation, the fluid then becomes birefringent. Both the magnetic field intensity and orientation can modulate the RI of magnetic fluids. The propagation constants and evanescent field absorption of the cladding modes are significantly influenced by varying RI of the surrounding magnetic fluids. Not only the magnetic intensity, field vector sensing can be realized owing to asymmetric interaction of magnetic fluids. [75] and [77] also designed magnetic field sensors based on different MOFs, though field vector were not

taken into account, they considered temperature compensating during magnetic field intensity measuring.

Table III concludes MOF electric and magnetic field sensors. Some of the sensors still have limitations, such as the LC infiltrated MOF electric field sensors can only respond to AC field, having response threshold, and the magnetic fluids causing high loss etc., more suitable materials may be discovered and integrated in the MOFs instead in the coming years. Fabricating the fiber instead with high transparency electro/magneto-optic material may be another solution, however, the electro-optic material are mostly crystals that cannot be thermally drawn. Integrating electro-optic crystal like $LiNbO_3$ into glass clad MOFs is a possible way but still difficult to realize. With the introduce of machine learning, electric/magnetic field sensors are enabled to measure intensity at different positions simultaneously or locate a filed [150].

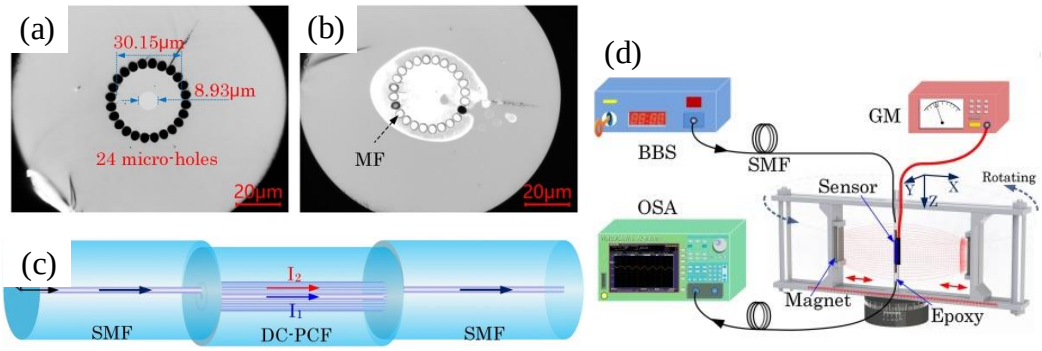


**Fig. 14** (a) Structure of the MOF [76]. (b) After infiltrated magnetic fluids in the MOF. (c) MZI based on the MF filled MOF. (d) Magnatic field sensing experimental setup.

**Table III. Summary of the MOF electric/magnetic field sensors**

| Ref. | Factor | Fiber | Principle | Performance |
|---|---|---|---|---|
| [23] | Electric field | SMPCF | Sagnac | 504 nm/kV/mm |
| [72] | | PMPCF | Polarization | ~20 dB/$kV_{rms}$/mm |
| [73] | | SMPCF | Coupling | 5.594 nm/V |
| [74] | Magnetic field | Side-Polished Hollow-Core fiber | Mach–Zehnder | 240 pm/mT; |
| [75] | | Bragg fiber | Anti-resonant | 86.43 pm/mT, |
| [76] | | DC-PCF | Mach–Zehnder | 114.5 pm/mT |
| [77] | | Exposed core fiber | Mach–Zehnder | −0.18 nm/mT |

*4.4 Humidity, Gas*

Humidity measurement is indispensable in environment monitoring for precise instrument, food industry, farming, or breath detecting. For fiber-based humidity sensors [79-86], in order to let the environment influence the optical transmission of fiber, the sensing structures are usually exposed and some humidity sensitive materials like $SnO_2$ [79, 80], PVA [81] or gelatin [82] are induced to enhance sensitivity and shorten response time. Structures include open end cavities which usually form F-P interferometers [80, 83] and side-exposed structures which can be realized by polishing [82], tapering [84], etching cladding [85], collapsing air-holes of PCFs [79, 81] or using specially designed MOFs, whose principles are alternating ambient RI, enhancing evanescent field and forming MZI. In [82], the single eccentric hole-assistant dual-core fiber (SEHADCF in Fig. 15(a)) had one core in the center and another core suspended in the side hole, they are the same in RI and size and close enough to each other so that light transmitting can couple between two wave guides. The researchers polished the fiber to expose the suspended fiber core. Humidity sensitive layer was coated on the polished surface after 15 coating processes and covered the suspended core which exposed to environment (Fig. 15(b)). After calculating the coupling length between two cores, the length of the fiber was precisely cut to 10.5 mm, which is odd times of the coupling length to achieve most obvious resonant dips on spectrum. They concluded that the resonant dip is weak when the film is thin, so they filled the open hole as much as possible to introduce strong a coupling. RI of gelatin decreases with increasing relative humidity, thus tunes the phase matching condition between two cores by changing the mode effective RI of the suspended core, causing shift of the coupling resonant dip. The sensor showed good stability, high sensitivity, fast response less than 3 seconds and also a low temperature crosstalk. Table IV lists the MOF based humidity sensors for comparison. Though the performance depends on the material to some extent, the exposed structure of MOF is an important part in these sensors.

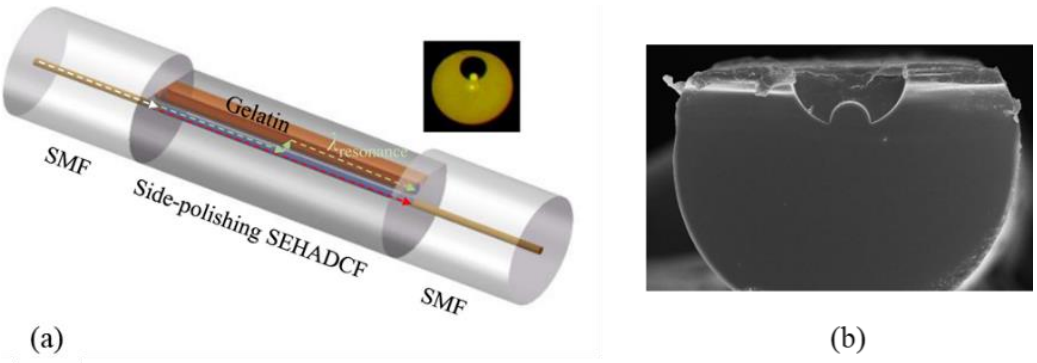


**Fig. 15** (a) Structure of the humidity sensor based on gelatin coated side-polished MOF (Inset: original unpolished fiber). (b) Image of the coated gelatin layer on the core. [82]

**Table IV. Summary of the MOF humidity sensors**

| Ref. | Fiber | Material | Principle | Performance |
|---|---|---|---|---|
| [79] | PCF | $SnO_2$ | Mach–Zehnder | 3 nm/%RH (20%-90%RH) |
| [81] | PCF | PVA | Mach–Zehnder | 40.9 pm/%RH (20%-95%RH) |
| [82] | SEHADCF | gelatin | Coupling | −7.005 nm/%RH (70%-90%RH) |
| [83] | Suspended tri-core fiber | chitosan | Fabry–Pérot | 81.05 pm/%RH (90%-95%RH) |
| [84] | Dual side-hole fiber | graphene oxide | Mach–Zehnder | − 0.142 nm/%RH (30%-60%RH) |
| [86] | G-PCF | -- | Mach–Zehnder | −0.077 dB/% RH (25%-80%RH) |

Fiber gas sensors which also need light interacting with environment have very similar structures to the humidity sensors. Not only gas sensors based on RI variation of the sensitive films exposed to gases such as polys for ammonia [87, 88] and graphene for hydrogen sulfide [89], the absorption based gas sensors also need structures allowing contact between light and gases. In [90], with the help of two sections of C-type fiber, gas can flow into the suspended ring core fiber (Fig. 16(a)(b)(c)), which had a higher index ring guiding light around the hollow center and surrounded by multiple small air holes. When $C_2H_2$ was pumped in with constant pressure balanced by $N_2$, the transmission drop of absorption lines is monitored to measure the $C_2H_2$ concentration

(Fig. 16(d)). The sensor responded well while the concentration is as low as 0.53%, far below the explosion limit of $C_2H_2$ which is about 2%. In this novel hollow MOF, the ring core let the light contact with gas as much as possible, shortens response time and enhances sensitivity which is expressed by the fraction of total power located in the air holes:

$$f = \int_{sample} Re(E_x H_y^* - E_y H_x^*) / \int_{total} Re(E_x H_y^* - E_y H_x^*)\, dx\, dy \qquad (7)$$

in which $E_x$, $E_y$, and $H_x$, $H_y$ are the electric and magnetic field components in transverse. The sensor setup is also relatively simple. Other structures like microstructured-core in PCF can also enhance the evanescent field interacting with the gases [92]. Hollow core PBG fibers or ARFs are often directly used in gas sensing based on principles such as direct absorption [93-95], wavelength modulation spectroscopy [97] and photothermal spectroscopy [98]. Since the light transmit in the gas infiltrated hollow core, the light-gas interaction efficiency is maximized and by specifically designing the hollow core fiber parameters, the transmission widow can be adjusted to cover the absorption peaks at different wavelengths to detect a specific gas [96]. In [97] 13 m of hollow core PCF was used to detect $C_2H_2$, having a limit of detection (LOD) less than 1 ppm. An LOD as low as 2 ppb for $C_2H_2$ detection system was carried out by W. Jin [98], in which gas was infiltrated in 10 m of hollow core PCF. Hollow core MOF based gas sensors can achieve very low LODs. The LOD is the most important gauge of gas sensor because some gases may be explosive or harmful. The hollow core fiber solved the problem of spatial optical-gas interaction that cannot be applied in practice sensing, however, the fibers in these sensing devices are still long, bending loss cannot be neglected if the fibers are winded in small diameter, which prevents further compaction of the sensors' size. Hollow core fiber with lower bending loss may be developed in coming years.

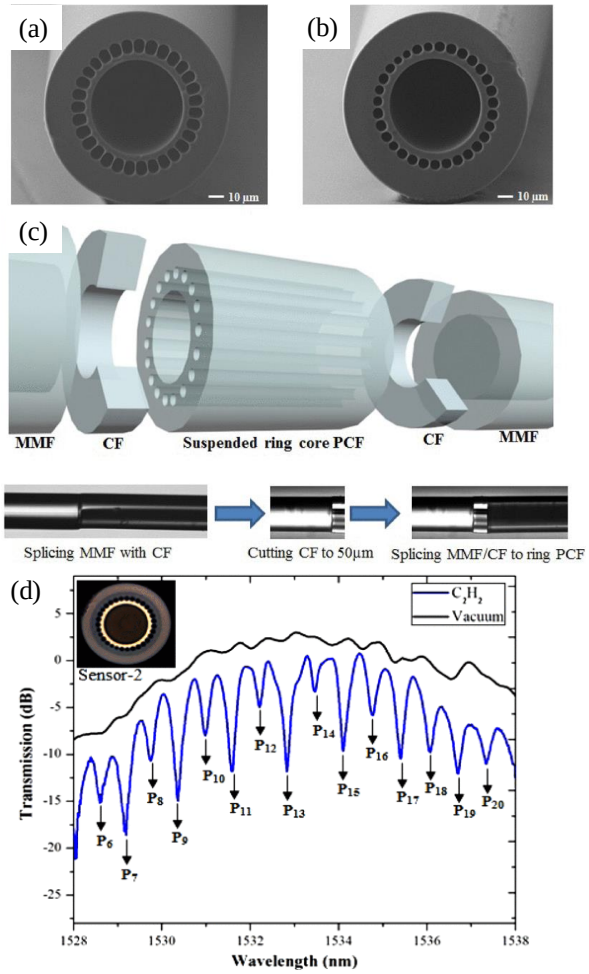


**Fig. 16** (a)(b) Structure of the ring core MOF used in [90]. (c) Gas was able to flow into the MOF through the C-type fiber. (d) Spectrum of the sensor in vacum and $C_2H_2$.

*4.5 RI, Analyte*

Optofluidics [99] which has become perspective in recent years because of the advantages such as fast response, high sensitivity and low detecting limit and its possibility to be applied in fields like health and disease diagnosis [139,140], is attracting numbers of researchers working on fiber optofluidics devices [100,101]. MOFs with micro channels provide a good platform for solutions to interact with light. Thus allowing the light transmitted in the fiber has a large overlap with the analytes and tailoring the fiber profile to match the required detection mechanism. The MOF RI sensor [27,102-104,146] is one of the most uses. RI sensing is the basic principle behind a great deal of fiber sensors. An RI sensor based on SPR for microfluidic chip was demonstrated by Z. Liu et al. [105]. Resonant occurs when the wave vector parallel to the metal surface $K = {}^{\omega}/_{c}\sqrt{\varepsilon_0}\sin\theta$ matches the surface plasmon wave $K_{sp} =$

$\omega/c\sqrt{\varepsilon_1\varepsilon_2/(\varepsilon_1+\varepsilon_2)}$, in which $\omega$ is angular frequency of light wave, $\theta$ is incidence angle, $\varepsilon_0$, $\varepsilon_1$, $\varepsilon_2$ are dielectric constant of the fiber, metal and surrounding. They first polished two sections of the eccentric dual core hollow microstructure fiber (MHF, Fig. 17(a)) forming grinding angles at the tips, then butt-coupled the two sections of polished fiber together with the help of a polarization maintaining fiber splicer, and finally coated three gold films to reflect the light transmitting in the side core to excite SPR on both external (zone 1) and internal channel (zone 2) (Fig. 17(b)), the incident angle of the external sensing and internal zone is 83° and 76° respectively. For a certain incident angle, resonant dips occur on the spectrum and vary with the RI of liquid sample in a range, thus realized RI sensing outside the fiber in zone 1 or inside the fiber hollow channel in zone 2. The sensitivity reached 5645 nm/RIU ranged from 1.333 to 1.385 in the internal channel which is an impressive performance among RI sensors. This RI sensor has potential to be integrated in fiber microfluidic chip system.

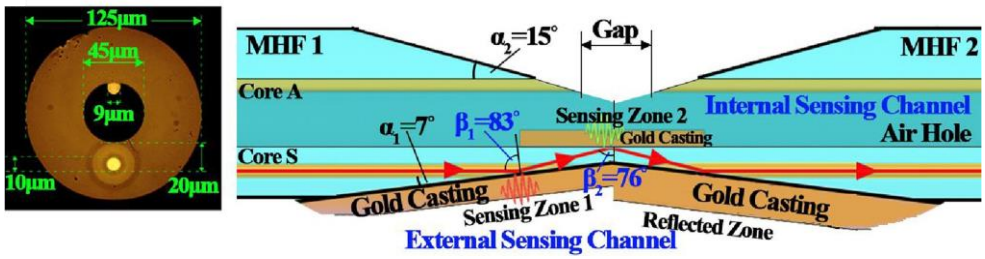


(a) (b)

**Fig. 17** (a) Structure of the MOF in [105]. (b) Structure of the SPR RI sensor based on the MOF and light transmission path in the sensor. SPR can be excited both on zone 1 and 2.

**Table V. Summary of the MOF RI sensor**

| Ref | Fiber | Principle | Performance |
|---|---|---|---|
| [27] | Exposed core MOF | Grating | 1.1 nm/RIU |
| [102] | Parallel channel fiber | Coupling | 3259 nm/RIU |
| [103] | Single Stress-Applying Fiber | Coupling | 30563 nm/RIU |
| [104] | Etched MOF | Mach–Zehnder | 2183.6 nm/RIU |
| [105] | Hollow MOF (two core) | SPR | 5645 nm/RIU |
| [112] | Expose core fiber | Sagnac | −3137 nm/RIU |
| [114] | Optofluidic channel PCF | Sagnac | 2849 nm/RIU |

The sensing abilities of MOF RI sensors are summarized in Table V. In addition to

the basic RI sensing, characterizing the RI of a specific liquid has also broadened the horizon of chemical and biochemical analyte sensing [106-111]. A. Zhang et al. realized trace detection of cadmium with a side open anti-resonant fiber in an interferometric setup [107]. V. Chaudhary et al. designed and simulated a PCF plasmonic biosensor for blood composition detection (Fig. 18) and pointed out the fabrication method of the PCF in reality [138]. X. Li et al. embedded the expose core fiber (ECF) (Fig. 19(a)) into a Sagnac interferometer obtaining a RI sensitivity of −3137 nm/RIU, and demonstrated the application of label-free biosensor by immobilizing biotin onto the fiber core which works as capturing probe for target streptavidin molecules, Fig. 19(b) describes the procedures of fiber surface functionalization and the bio detection mechanism. The bio layer thickness on the core changes effective RI of x and y polarization mode of the fiber resulting in wavelength shift [112]. Then in 2022, X. Li et al. tapered the same expose core fiber to excite $LP_{11}$ mode and formed an MZI, resulting in a RI sensitivity of 1771 nm/RIU. This time probe DNA (pDNA) was immobilized on the exposed side to detect the complementary DNA (cDNA), having a sensitivity of 0.0618 nm/nM and a detection limit of 0.31 nM [113]. A fiber with built-in microstructured optofluidic channels was produced by N. Zhang et al. [114]. The fiber was specially designed for their biochemical sensing research; its schematic is shown in Fig. 20(a). The fiber structure is novel, which was fabricated by the same stack and draw method of fabricating a PCF but leaving one-sixth of the structure in cladding empty forming a fluidic channel. They discussed in-line absorption sensing and RI sensing characteristics of the fiber based on Sagnac interferometer and finally carried out human cardiac troponin T (cTnT) measurement based on the biological binding of antibody and antigen immobilized on the surface of expose core in the channel. Fig. 20(b) illustrated the molecule binding step by step, as the cTnT attached to the antibody, the interference dip red shift with increasing concentration (Fig. 20(c)). The sensor has a linear response above 1 ng mL-1, which is able to able to detect cTnT protein as low as 1 ng $mL^{-1}$ (Fig. 20(d)).

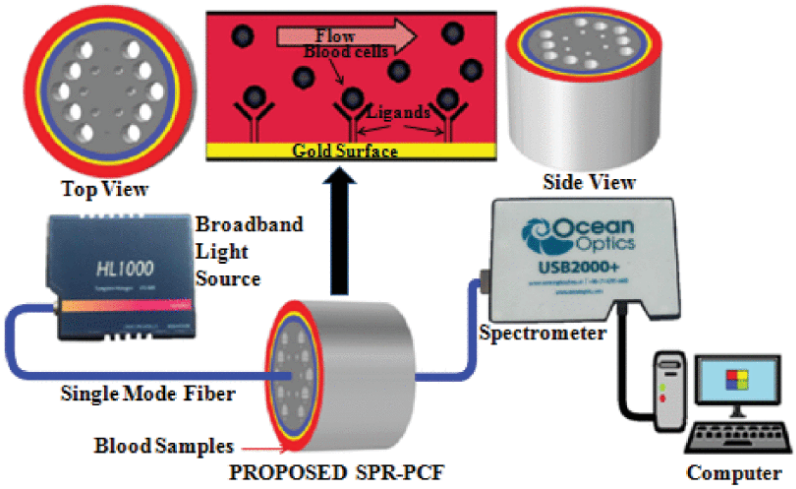


**Fig. 18** PCF plasmonic biosensor for blood composition detection [138].

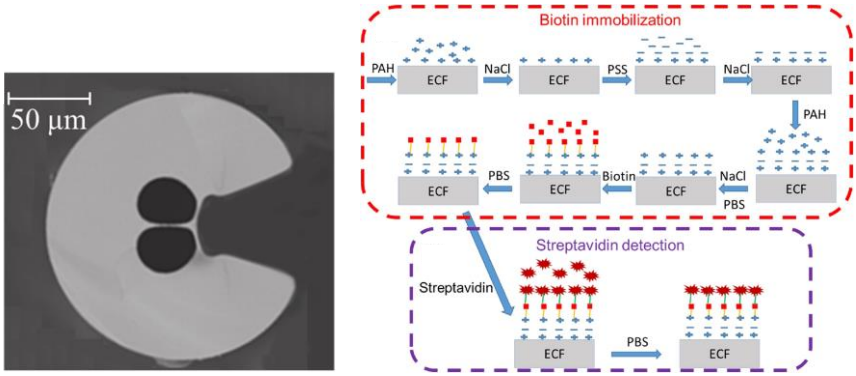


(a) (b)

**Fig. 19** (a) The expose core fiber used in [112] and [113]. (b) Surface-functionalization and bio-sensing.

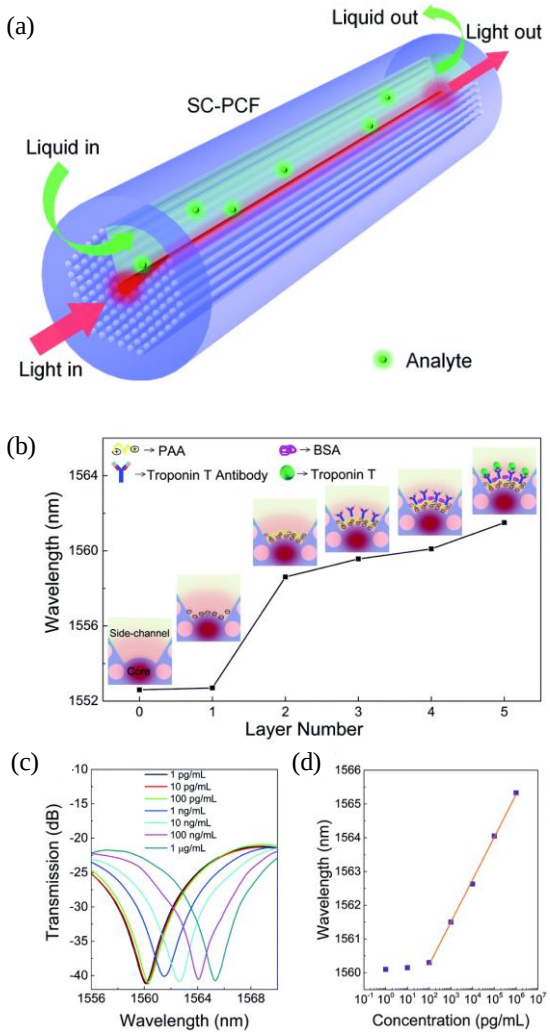


**Fig. 20** (a) Sensing structure of the built-in microstructured optofluidic channel PCF in [114]. (b) Immobilize antibody and antigen on the core in the optofluidic channel to realize human cTnT sensing. (c) Shift of the transmission spectra to the binding effect of different concentrations of the cTnT antigen. (d) Wavelength shifts

Chemical and biochemical fiber sensor is attracting more research interests in recent years, substance like p-Cresol, Aflatoxins B1 and creatinine etc. can be detected [141-145], optical detection of the substance is prospective for its advantages such as low LOD and fast response. Besides interferometer and SPR, chemical/biochemical sensing based on absorption, fluorescence and Raman spectroscopy also widely use fibers with micro channels [135,136]. The treatments on fiber like deposition of sensitive films or particles etc. are important procedures, sometimes depositing in a small size micro-channel is still challenging. Other than that, the analyte insertion method into the fiber channel is also a key point need to be considered in designing the

optofluidic devices, drilling holes on capillary or use the C-type fiber in Fig. 16(c) are feasible solutions. Integrating the MOF with microfluidic chips will make sensing more convenient, as well as improving the stability and repeatability of the sensor. MOFs are good carriers for the interaction between the analyte and light, they also provide reaction channels for substance which will accelerate sensor response and realize real-time detection. For now, fiber biosensors are still mostly applied in vitro detection, more applies in vivo detection may be possible if the MOF are safer to be inserted into body. The liquid consumption in MOF micro channels are very low, which is an obvious advantage in biochemical and toxic substances sensing. Biosensors will also be boosted by the development of nanomaterial [149], the nanomaterial is ultra-thin which benefits coating on the MOFs and enhance the sensing capabilities. Innovating the existing diagnosis and detection with optical fiber biosensor technology is expected to achieve disruptive innovative results and realize clinical application.

**5. Prospect and summary**

Sensing application is one of the main purposes in designing and fabricating the MOFs. MOF sensors are mostly based on the special design which can improve the influence of factors on transmission properties, or provide a platform to carry other sensitive materials. Besides later inducing sensitive materials, integrating the materials initially are excellent ideas. For example, fibers are made of materials sensitive to humidity themselves [130]. Less complicated post-treatment produces on MOFs are needed compared with conventional fiber when fabricating the senor probe, which will promote mass production.

Fabricating the fiber with unconventional materials instead of silica further broadens the application field. The existing examples are polymer or plastic fibers, which have good affinity with living things, are safer to be implanted in human or animal bodies to realize real time sensing on livings [115,116]. Polymer fibers are also super elastic, therefore can be used in wearable devices [117-119]. MOFs made of soft glass (whose transition temperatures are much lower than silica glass) such as lead silicate, tellurite and chalcogenide glass which are more often used to generate supercontinnum [120], contrary to the silica fiber whose loss is low only at near IR wavelength, they usually have wide transparency window from UV to Mid-IR. Soft

glass MOFs can be well applied in chemical or gas sensing since they can generate and transmit the wavelengths that fully cover the chemical and gas absorption line in Mid-IR.

Other than that, microstructure multi-material and multi-functional fibers are attracting more attention from researchers. Researchers have managed to integrate different materials in fiber, the key to fabricate multi-material fibers is to make sure the melting/softening temperatures of different materials are close, or melting/softening temperature of the inner material is lower than the outer so the outer amorphous material can maintain the fiber structure during drawing. Metals induced in fibers are good candidates to excite SPR for sensing applications [121]. Metals wires can be introduced by directly drawing in the fiber preform [123] or later pressuring melted metals into the air holes [122]. However MOFs with thin metals films deposited on the inner air holes, sensors based on which have been proved to possess extremely high sensitivities in many simulation researches [124,125], are still not easily achievable in experimental practice.

The ability to integrate different materials into the optical fibers provides the fibers with multiple novel functions. Besides metals, integrating many other materials such as different kinds of polymers, crystals, semiconductors in the fibers and making the fiber multi-functional is the state of the art of research on microstructured fibers [126]. Fibers which contain polymer, metal and composite materials were designed. The waveguides, electrodes and micro channels integrated in the fiber enabled electrical, chemical and mechanical signaling simultaneously. Electrical, optical and microfluidic measurements have testified the use of the fiber as neural probes on brain [127]. Spatially expandable multifunctional fiber probes which enables manipulation and mapping of brain activities in three-dimensional is further developed [128]. Lab-in-Fiber is one of the most popular topic in recent and many researchers have transferred their attention to the designs, developments and applications of fiber gas, chemical and biomecical sensing devices since they are prospective in fields like public health, disease diagnosis, smart medical device and environment science etc. [147,148]. The research on Lab-in-fiber technology in which the multi-functional MOFs play important roles will still be popular in next few years.

In general, in recent and future researches, the most likely developing direction may be the innovation on the materials and designs of the MOFs and broaden their functionality in sensing fields. Not only the examples we have discussed, combining the MOF with novel materials (such as 2D material graphene [131]) to improve sensing performance and simplify the sensor setup is also becoming possible. Crystals and fluorescent materials sensitive to physical fields or chemical substances are also potential candidates to be integrated into MOFs to realize sensing.

And finally, as the advantages of MOFs in sensing applications are explained in detail above, however compared with conventional fibers, the disadvantages are difficulties in fiber fabrication and splicing connection with other fibers. Other challenges include the productization of finished senor, as well as the transmission loss and cost which are faced by almost all fiber sensing plans currently. Those are the issues need to be addressed urgently before these MOF sensors widely applied in real life. MOFs with interesting designs have resulted in amazing properties and expanded the measurement and sensing fields. MOF sensors are believed to have wider uses in practice. MOFs are also developing novel functionalities and opening new world of applications.

## Acknowledgments

This work was funded by the National Natural Science Foundation of China (Grant No. 51907017), Hebei Natural Science Foundation (Grant No. F2020501040), the Fundamental Research Funds for the Central Universities of China (Grant No. N2123012).

## References

[1] S. Rezapour, N. Jiang, E. Ozturk, A. Yetisen and S. Tasoglu. Biomedical optical fibers, Lab Chip. 21 (4) (2021) 627-640.

[2] C. Leung, K. Wan, D. Inaudi. X. Bao, W. Habel, Z. Zhou, J. Ou, M. Ghandehari, H. Chung Wu and M. Imai, Review: optical fiber sensors for civil engineering applications, Mater Struct 48 (2015) 871–906.

[3] B. Lee, Review of the present status of optical fiber sensors, Opt. Fiber Technol. 9 (2) (2003) 57-79.

[4] C. Jauregui, J. Limpert. and A. Tünnermann, High-power fibre lasers, Nature Photon 7 (8) (2013) 861–867.

[5] L. Zhang, and C. Yang. Polarization splitter based on photonic crystal fibers, Opt. Express 11 (9) (2003) 1015-1020.

[6] J. Dudley, G. Genty, and S. Coen, Supercontinuum generation in photonic crystal fiber, Rev. Mod. Phys. 78 (2006) 1135.

[7] D. Mao, C. Guan, and L. Yuan, 1×4 coupler based on all solid five-core photonic crystal fibers, Opt. Commun., 284(19) (2011) 4460-4464.

[8] P. Mach, M. Dolinski, K. W. Baldwin, and J. A. Rogers, Tunable microfluidic optical fiber, Appl. Phys. Lett 80(23) (2002) 4294-4296.

[9] P. Russell. Photonic crystal fibers. Science 299 (5605) (2003) 358-362.

[10] M. Habib, J. Antonio-Lopez, C. Markos, A. Schülzgen, and R. Amezcua-Correa, Single-mode, low loss hollow-core anti-resonant fiber designs, Opt. Express 27 (2019) 3824-3836.

[11] K. Yoshida, T. Morikawa, Fabrication and characterization of side-hole single-mode optical fibers, Opt. Fiber Technol 2 (3) (1996) 285-290.

[12] O. Frazão, R. Silva, M. Ferreira, J. Santos, and A. Lobo Ribeiro, Suspended-core Fibers for Sensing Applications, Photonic Sens. 2 (2) (2012) 118–126.

[13] W. Reeves, J. Knight, P. Russell and P. Roberts, Demonstration of ultra-flattened dispersion in photonic crystal fibers, Opt. Express 10 (14) (2002) 609-613.

[14] K. Hansen. Dispersion flattened hybrid-core nonlinear photonic crystal fiber. Opt. Express 11 (13), (2003) 1503-1509.

[15] P. Roberts, F. Couny, H. Sabert, B. Mangan, D. Williams, L. Farr, M. Mason, A. Tomlinson, T. Birks, J. Knight, and P. Russell, Ultimate low loss of hollow-core photonic crystal fibres, Opt. Express 13 (1) (2005) 236-244.

[16] A. Argyros, T. Birks, S. Leon-Saval, C. Cordeiro, and P. Russell, Guidance properties of low-contrast photonic bandgap fibres, Opt. Express 13 (2005) 2503-2511.

[17] W. Henry, Evanescent field devices: a comparison between tapered optical fibres and polished or D-fibres, Opt. Quant Electron 26 (1994) S261–S272.

[18] J. Ju, W. Jin and M.S. Demokan. Properties of a highly birefringent photonic crystal fiber, IEEE Photon. Technol. Lett. 15 (10) (2003) 1375-1377.

[19] C. Zhang, H. Zhu, and B. Shi, Role of the interface between distributed fibre optic strain sensor and soil in ground deformation measurement, Sci. Rep. 6 (1) (2016) 36469.

[20] L. Kong, J. Jin, W. Cai, F. Gao, K. Ma, J. He, N. Song, C. Zhang, High precision interferometric fiber optical gyroscopes based on photonic-crystal fiber for space application, IEEE Aerospace Conference (50100) (2021) 1-7.

[21] M. Ramakrishnan, G. Rajan, Y. Semenova and G. Farrell, Overview of fiber optic sensor technologies for strain/temperature sensing applications in composite materials, Sensors (Basel) 16 (1) (2016).

[22] D. Sharma, A. Sharma and S. Tripathi, Cladding mode coupling in long-period gratings in index-guided microstructured optical fibers, Appl. Phys. B 123 (187) (2017).

[23] P. Xue, Q. Liu, Z. Wu, Q. Wu, C. Zhao, W. Ng , R. Fu , and R. Binns, Electrically tuning characteristics of LC selectively infiltrated PCF Sagnac interferometer, IEEE Photon. Technol. Lett. 33 (13) (2021).

[24] Q. Liu, L. Xing, S. Yan, L. Lv, and Z. Liu, Sensing characteristics of photonic crystal fiber Sagnac interferometer based on novel birefringence and Vernier effect, Metrologia 57 (3) (2022) 035002.

[25] Z. Wang, W. Zhang, X. Liu, M. Li, X. Lang, R. Singh, C. Marques, B. Zhang, S. Kumar, Novel optical fiber-based structures for plasmonics sensors, Biosensors. 12 (2022) 1016.

[26] B. Wu, Y. Lu, C. Hao, L. Duan, M. Musideke, and J. Yao, A photonic crystal fiber sensor based on differential optical absorption spectroscopy for mixed gases detection, Optik 125 (12) (2014) 2909-2911.

[27] S. Warren-Smith and T. Monro, Exposed core microstructured optical fiber Bragg gratings: refractive index sensing, Opt. Express 22 (2), 2014.

[28] P. Zhang, M. Tang, F. Gao, B. Zhu, Z. Zhao, L Duan, S. Fu, J. Ouyang, H. Wei, P. Shum, and D. Liu. Simplified hollow-core fiber-based Fabry-Perot interferometer with modified vernier effect for highly sensitive high-

temperature measurement, IEEE Photon. J. 7 (1) (2015) 1-10.

[29] S. Sulejmani, C. Sonnenfeld, T. Geernaert, G. Luyckx, D. Hemelrijck, P. Mergo, W. Urbanczyk, K. Chah, C. Caucheteur, P. Mégret, H. Thienpont and F. Berghmans. Shear stress sensing with Bragg grating-based sensors in microstructured optical fibers, Opt. Express 21 (17) (2013) 20404-20416.

[30] K. Ahmed, B. Paul, S. Chowdhury, M. Islam, S. Sen, M. Islam, S. Asaduzzaman, A. Newaz Bahar and M. Miah, Dataset on photonic crystal fiber based chemical sensor, Data in Brief 12 (2017) 227-233.

[31] A. Rifat, K. Ahmed, S. Asaduzzaman, B. Paul and R. Ahmed. Development of Photonic Crystal Fiber-Based Gas/Chemical Sensors. Computational Photonic Sensors (2015) 287-317.

[32] M. Rachana, I. Charles, S. Swarnakar, S. Krishna, S. Kumar, Recent advances in photonic crystal fiber-based sensors for biomedical applications, Opt. Fiber Technol. 74 (2022) 103085.

[33] Libo Yuan, Building a lab-in/on-fiber, Proc. SPIE 9655, Fifth Asia-Pacific Optical Sensors Conference (2015) 96552C.

[34] S. Pissadakis, Lab-in-a-fiber sensors: A review, Microelectron. Eng. 217 (2019) 111105.

[35] E. Chillcce, C. Cordeiro, R. Ramos, B. Honrio, E. Rodriguez, G. Jacob, C. Cruz, C. Cesar and L. Barbosa, Development of soft-glasses photonic crystal fiber made by stacking-and-draw technique, Optical Components and Materials IV 6469 (2017) 64690U.

[36] B. Kaur, S. Kumar, B. Kaushik, Advances in photonic crystal fiber: sensing and supercontinuum generation applications, 72 (2022) 102982.

[37] M. Tse, Z. Liu, L. Cho, C. Lu, P. Wai, and H. Tam, Superlattice microstructured optical fiber, Materials 7 (6) (2014) 4567–4573.

[38] X. Feng, A. Mairaj, D. Hewak, A Mairaj, D. Hewak and T. Monro. Nonsilica glasses for holey fibers, IEEE J. Lightwave Technol. 23 (6) (2006) 2046-2054.

[39] C. Strutynski, O. Mouawad, J. Picot-Clémente, P. Froidevaux, F. Désévédavy, G. Gadret, J. Jules, B. Kibler and F. Smektala, Optical aging observation in suspended core tellurite microstructured fibers under atmospheric conditions, Opt. Fiber Technol. 38 (2017) 154-159.

[40] S. Warren-Smith, R. Kostecki, L. Nguyen, and T. Monro, Fabrication, splicing, Bragg grating writing, and polyelectrolyte functionalization of exposed-core microstructured optical fibers, Opt. Express 22 (24) (2014) 29493.

[41] T. Yuan, X. Zhang, Q. Xia, Y. Wang, and L. Yuan, A twin-core and dual-hole fiber design and fabrication, IEEE J. Lightwave Technol. 39 (12) (2021) 4028-4033.

[42] P. Falkenstein, C. Merritt and B. Justus, Fused preforms for the fabrication of photonic crystal fibers, Opt. Lett. 29 (16) (2004) 1858-1860.

[43] G. Zhou, Z. Hou, S. Li and L. Hou, Fabrication of glass photonic crystal fibers with a die-cast process, Appl. Opt. 45 (18) (2006) 4433-4436.

[44] V. Kumar, A. George, W. Reeves, J. Knight, P. Russel, F. Omenetto and A. Taylor, Extruded soft glass photonic crystal fiber for ultrabroad supercontinuum generation, Opt. Express 10 (25) (2002) 1520-1525.

[45] M. Becker, M. Werner, O. Fitzau, D. Esser, J. Kobelke, A. Lorenz, A. Schwuchow, M. Rothhardt, K. Schuster, D.Hoffmann, H. Bartelt, Laser-drilled free-form silica fiber preforms for microstructured optical fibers, Opt. Fiber Technol. 9(5) (2013) 482-485.

[46] K. Cook, J. Canning, S. Leon-Saval, Z. Reid, M. Hossain, J. Comatti, Y. Luo and G. Peng, Air-structured optical fibre drawn from a 3D-printed preform, Opt. Lett 40 (17) (2015) 3966.

[47] Q. Zhao, F. Tian, X. Yang, S. Li, J. Zhang, X. Zhu, J. Yang, Z. Liu, Y. Zhang, T. Yuan and L. Yuan, Optical fibers with special shaped cores drawn from 3D printed preforms, Optik 133 (2017) 60-65.

[48] W. Talataisong, R. Ismaeel, T. Marques, S. Mousavi, M. Beresna, M. Gouveia, S. Reza Sandoghchi, T. Lee, C.

Cordeiro and G. Brambilla. Mid-IR Hollow-core microstructured fiber drawn from a 3D printed PETG preform. Sci. Rep. 8 (2018) 8113.

[49] Y. Chu, X. Fu, Y. Luo, J. Canning, Y. Tian, K. Cook, J. Zhang, and G. Peng, Silica optical fiber drawn from 3D printed preforms, Opt. Lett 44 (21) (2019) 5358-5361.

[50] C. Cordeiro, A. Ng and H. Ebendorf-Heidepriem, Ultra-simplifed Single-Step Fabrication of Microstructured Optical Fiber, Sci Rep 10 (2020) 9678.

[51] C. Smith, N. Venkataraman, M. Gallagher, D. Müller, J. West, N. Borrelli, D. Allan and K. Koch. Low-loss hollow-core silica/air photonic bandgap fibre, Nature 424 (2003) 657–659.

[52] W. Ding, Y. Wang, S. Gao, M. Wang, and P. Wang, Recent progress in low-loss hollow-core anti-resonant fibers and their applications, IEEE J. Sel. Top. Quant. 26 (4) (2020) 4400312.

[53] W. Ni, C. Yang, Y. Luo, R. Xia, P. Lu, D. Hu, S. Danto, P. Shum and L. Wei, Recent Advancement of Anti-Resonant Hollow-Core Fibers for Sensing Applications, Photonics 8 (4) (2021) 128.

[54] N. Litchinitser, A. Abeeluck, C. Headley, and B. Eggleton, Antiresonant reflecting photonic crystal optical waveguides, Opt. Lett. 27 (18) (2002) 1592-1594.

[55] Q. Liu, L. Xing, Z. Wu; Y. Fu, S. Li, P. Xue, W. Ng, Q. Wu, Cascaded sagnac loops embedded with two polarization maintaining photonic crystal fibers for highly sensitive strain measurement, IEEE T. Instrum. Meas. 70 (2021) 7002309.

[56] Z. Liu, C. Wu, M. Tse, and H. Tam, Fabrication, Characterization, and sensing, applications of a high-birefringence, suspended-core fiber, IEEE J. Lightwave Technol. 32 (11) (2014) 2113-2122.

[57] K. Qureshi, Z. Liu, H. Tam and M. Zia, A strain sensor based on in-line fiber Mach–Zehnder interferometer in twin-core photonic crystal fiber, Opt. Commun. 309 (15) (2013) 68-70.

[58] G. Mao, T. Yuan, C. Guan, J. Yang, L. Chen, Z. Zhu, J. Shi, and L. Yuan, Fiber Bragg grating sensors in hollow singleand two-core eccentric fibers, Opt. Express 25(1) (2017) 144-150.

[59] D. Budnicki, I. Parola, Ł. Szostkiewicz, K. Markiewicz , Z. Hołdy ´nski , G. Wojcik, M. Makara, K. Poturaj, M. Kukli ´nska, P. Mergo , M. Napierała, and T. Nasiłowski, All-fiber vector bending sensor based on a multicore fiber with asymmetric air-hole structure, IEEE J. Lightwave Technol 38 (23) (2020) 6685-6690.

[60] A. Anuszkiewicz, T. Martynkien, P. Mergo, M. Makara, and W. Urbanczyk, Sensing and transmission characteristics of a rocking filter fabricated in a side-hole fiber with zero group birefringence, Opt. Express 21 (10) (2013) 12657-12667.

[61] J. Osório, G. Chesini, V. Serrão, M. Franco and C. Cordeiro, Simplifying the design of microstructured optical fibre pressure sensors, Sci. Rep. 7 (2017) 2990.

[62] O. Frazão, R. Silva, J. Kobelke, and K. Schuster, Temperature- and strain-independent torsion sensor using a fiber loop mirror based on suspended twin-core fiber, Opt. Lett. 35 (16) (2010) 2777-2779.

[63] W. Chen, S. Lou, L. Wang, H. Zou, W. Lu, and S. Jian, Highly sensitive torsion sensor based on Sagnac interferometer using side-leakage photonic crystal fiber, IEEE Photonic Tech L. 23 (21) (2011) 1639-164.

[64] J. Li, Boyao Li, C. Xia, Z. Hou and G. Zhou, High order modes suppression and manipulation in six-holes helical chiral microstructure fiber, Opt. Fiber Technol. 61 (2021) 102445.

[65] W. Shin, Y. Lee, B. Yu, Y. Noh and K. Oh, Spectral characterization of helicoidal long-period fiber gratings in photonic crystal fibers, Opt. Commun. 282 (2009) 3456–3459.

[66] J. Zhao, Y. Zhao, L. Bai and Y. Zhang, Sagnac interferometer temperature sensor based on microstructured optical fiber filled with glycerin, Sens. Actuator A Phys. 314 (2020) 112245.

[67] E. Reyes-Vera, C. Cordeiro, and P. Torres, Highly sensitive temperature sensor using a Sagnac loop interferometer based on a side-hole photonic crystal fiber filled with metal, Appl. Opt 56 (2) (2017) 156-162.

[68] Y. Liang, H. Zhang, B. Huang, B. Liu, W. Lin, J. Sun and D. Wang, Ultrahigh-sensitivity temperature sensor

based on resonance coupling in liquid-infiltrated side-hole microstructured optical fibers, Sens. Actuator A Phys. 334 (2022) 113358.

[69] S. Liu, Y. Wang, M. Hou, J. Guo, Z. Li, and P. Lu, Anti-resonant reflecting guidance in alcohol-filled hollow core photonic crystal fiber for sensing applications, Opt. Express 21 (25) (2013) 31690-31697.

[70] R. Gao, D. Lu, J. Cheng and Z. Qi, Simultaneous measurement of refractive index and flow rate using graphene-coated optofluidic anti-resonant reflecting guidance, Opt. Express 25 (23) (2017) 28731-28742.

[71] E. Davies, P. Christodoulides, G. Florides, and K. Kalli, Microfluidic flows and heat transfer and their influence on optical modes in microstructure fibers, Materials 7 (11) (2014) 7566-7582.

[72] S. Mathews, G. Farrell and Y. Semenova, All-fiber polarimetric electric field sensing using liquid crystal infiltrated photonic crystal fibers, Sens. Actuator A Phys. 167 (2011) 54–59.

[73] Y. Huang, Y. Wang, L. Zhang, Y. Shao, F. Zhang, C. Liao, and Y. Wang, Tunable electro-optical modulator based on a photonic crystal fiber selectively filled with liquid crystal, IEEE J. Lightwave Technol. 37 (9) (2019) 1903-1908.

[74] R. Xu, G. Niu, Y. Xue, C. Ke, H. Deng, S. Deng, M. Chen, and L. Yuan, An all-optical vector magnetic field sensor based on magnetic fluid and side-polished hollow-core optical fiber, IEEE Sens. J. 21 (19) (2021) 21410-21416.

[75] Y. Huang, H. Qiu, C. Deng, Z. Lian, Y. Yang, Y. Yu, C. Hu, Y. Dong, Y. Shang, X. Zhang, and T. Wang, Simultaneous measurement of magnetic field and temperature based on two anti-resonant modes in hollow core Bragg fiber, Opt. Express 29 (20) (2021) 32208-32219.

[76] J. Yin, S. Ruan, T. Liu, J. Jiang, S. Wang, H. Wei and P. Yan, All-fiber-optic vector magnetometer based on nano-magnetic fluids filled double-clad photonic crystal fiber, Sensors and Actuators B: Chemical, Sens. Actuators B Chem. 238 (2017) 518–524.

[77] Q. Yu, X. Li, X. Zhou, N. Chen, S. Wang, F. Li, R. Lv, L. Nguyen, S. Warren-Smith, and Y. Zhao, Temperature Compensated Magnetic Field Sensor Using Magnetic Fluid Filled Exposed Core Microstructure Fiber, IEEE T. Instrum. Meas. 71 (2022) 7004408.

[78] L. Wei, T. Alkeskjold, and A. Bjarklev, Compact design of an electrically tunable and rotatable polarizer based on a liquid crystal photonic bandgap fiber, IEEE Photonic Tech. L. 21 (21) (2009) 1633-1635.

[79] D. Lopez-Torres, C. Elosua, J. Villatoro, J. Zubia, M. Rothhardt, K. Schuster and F. Arregui, Enhancing sensitivity of photonic crystal fiber interferometric humidity sensor by the thickness of $SnO_2$ thin films, Sens. Actuators B Chem. 251 (2017) 1059–1067.

[80] A. Lopez Aldaba, D. Lopez-Torres, C. Elosuaa, J. Auguste, R. Jamier, P. Roy, F. Arregui and M. Lopez-Amo, $SnO_2$-MOF-Fabry-Perot optical sensor for relative humidity measurements, Sens. Actuators B Chem. 257 (2018) 189–199.

[81] T. Li, X. Dong, C. Chiu Chan, K. Ni, S. Zhang, and P. Shum, Humidity Sensor With a PVA-Coated Photonic Crystal Fiber Interferometer, IEEE Sens. J. 13 (6) (2013) 2214-2216.

[82] J. Yang, C. Guan, Z. Yu, M. Yang, J. Shi, P. Wang, J. Yang, L. Yuan, High sensitivity humidity sensor based on gelatin coated side-polished infiber directional coupler, Sens. Actuators B Chem. 305 (2020) 127555.

[83] A. Shrivastav, D. Gunawardena, Z Liu and H. Tam, Microstructured optical fiber based Fabry–Pérot interferometer as a humidity sensor utilizing chitosan polymeric matrix for breath monitoring, Sci. Rep. 10 (2020) 6002.

[84] J. Fu, Y. Xu, M. Xu, L. Abbas, A. Zhou, Highly sensitive humidity sensor based on tapered dual side-hole fiber, Optik 261 (2022) 169183.

[85] C. Liu, F. Liu, H. Shen, Z. Dong, J. Zhou, G. Zhang, Z. Wei, F. Wang, C. Tan and H. Meng, Relative humidity sensor based on corrosive seven-core fiber coated with graphene oxide, Opt. Eng. 60 (11) (2021) 117105-1-

117105-9.

[86] P. Zhang, H. Yang, K. Lim, H. Ahmad, Q. Rong, Q. Tian and X. Ding, Temperature-independent hygrometry using micromachined photonic crystal fiber, Appl. Opt. 57 (15) (2018) 4237-4244.

[87] A. Shrivastav, G. Sharma, A. Rathore, and R. Jha, Hypersensitive and selective interferometric nose for ultratrace ammonia detection with fast response utilizing PANI@$SnO_2$ nanocomposite, ACS Photonics 5 (2018) 4402−441.

[88] X. Huang, X. Li, J. Yang, C. Tao, X. Guo, H. Bao, Y. Yin, H. Chen and Y. Zhu, An in-line Mach-Zehnder interferometer using thin-core fiber for ammonia gas sensing with high sensitivity, Sci. Rep. 7 (2017) 44994.

[89] X. Feng, W. Feng, C. Tao, D. Deng, X. Qin, and R. Chen, Hydrogen sulfide gas sensor based on graphene-coated tapered photonic crystal fiber interferometer, Sens. Actuators B Chem. 247 (2017) 540-545.

[90] S. Kassani, R. Khazaeinezhad, Y. Jung, J. Kobelke, and K. Oh, Suspended ring-core photonic crystal fiber gas sensor with high sensitivity and fast response, IEEE Photonics J. 7 (1) (2015) 2700409.

[91] S. Kassani, J. Park, Y. Jung, J. Kobelke, and K. Oh, Fast response in-line gas sensor using C-type fiber and Ge-doped ring defect photonic crystal fiber, Opt. Express 21 (12) (2013) 14074-14083.

[92] G. Mishra, D. Kumar, V. Chaudhary and S. Kumar, Design and Sensitivity Improvement of Microstructured-Core Photonic Crystal Fiber Based Sensor for Methane and Hydrogen Fluoride Detection, IEEE Sens. J. 22 (2) (2022) 1265-1272.

[93] C. Yao, S. Gao, Y. Wang, P. Wang, W. Jin , and W. Ren, Silica hollow-core negative curvature fibers enable ultrasensitive mid-infrared absorption spectroscopy, IEEE J. Lightwave Technol. 38 (7) (2020) 2067-2072.

[94] R. Wynne.; B. Barabadi, K. Creedon and A. Ortega, Sub-minute response time of a hollow-core photonic bandgap fiber gas sensor. IEEE J. Lightwave Technol. 27 (2009) 1590–1596.

[95] C. Yao, L. Xiao, S. Gao, Y. Wang, P. Wang, R. Kan, W. Jin. and W. Ren, Sub-ppm CO detection in a sub-meter-long hollow-core negative curvature fiber using absorption spectroscopy at 2.3 μm, Sens. Actuat. B Chem. 303 (2020) 127238.

[96] R. Yu, Y. Chen, L. Shui and L. Xiao, Hollow-Core Photonic Crystal Fiber Gas Sensing, Sensors 20 (2020) 2996.

[97] F. Yang, W. Jin, W, Y. Cao, H. Ho and Y. Wang, Towards high sensitivity gas detection with hollow-core photonic bandgap fibers, Opt. Express 22 (2014) 24894–24907.

[98] W. Jin, Y. Cao, F. Yang and H. Ho, Ultra-sensitive all-fibre photothermal spectroscopy with large dynamic range. Nat. Commun. 6 (2015) 6767.

[99] D. Psaltis, S. Quake and C. Yang. Developing optofluidic technology through the fusion of microfluidics and optics. Nature 442 (7101) (2016) 381-386.

[100] T. Yuan, X. Yang, Z. Liu, J. Yang, S. Li, D. Kong, X. Qi, W. Yu, Q. Long and L. Yuan, Optofluidic in-fiber interferometer based on hollow optical fiber with two cores, Opt. Express 25 (15) (2017) 18205-18215.

[101] T. Yuan, X. Zhang, Q. Xia, Y. Wang and L. Yuan, Design and fabrication of a functional fiber for micro flow sensing, IEEE J. Lightwave Technol. 39 (1) (2021) 290-294.

[102] H. Lee, M. Schmidt, P. Uebel, H. Tyagi, N. Joly, M. Scharrer and P. Russell, Optofluidic refractive-index sensor in step-index fiber with parallel hollow micro-channel, Opt Express 19 (9) (2011) 8200-8207.

[103] S. Xu, W. Chang, Y. Luo, W. Ni, Y. Zheng, L. Wei, Z. Xu, Z. Lian, Y. Zhang, Y. Huang and P. Shum, Ultrasensitive Broadband Refractometer Based on Single Stress-Applying Fiber at Dispersion Turning Point, IEEE J. Lightwave Technol. 39 (8) (2021) 2528-2535.

[104] B. Dai, X. Shen, X. Hu, L. Yang, H. Li, J. Peng and J. Li, Temperature-Insensitive Refractive Index Sensor with Etched Microstructure Fiber, Sensors, 19 (17) (2019) 3749.

[105] Z. Liu, X. Yang, Y. Zhang, Y. Zhang, Z. Zhu, X. Yang, J. Zhang, J. Yang and L. Yuan, Hollow fiber SPR sensor

available for microfluidic chip, Sens. Actuators B Chem. 265 (2018) 211–216.

[106] M. Calcerrada1, C. Garc´ıa-Ruiz1, and M. Gonzalez-Herraez, Chemical and biochemical sensing applications of microstructured optical fiber-based systems, Laser Photonics Rev. 9 (6) (2015) 604–627.

[107] A. Zhang, Z. Liu, Q. Tu, Q. Ma, H. Zeng, Z. Deng R. Jiang, Z. Mo, J. Liu, C. Xia, N. Zhao, Z. Hou, X. Huang and G. Zhou, Trace detection of cadmium (II) ions based on an air-hole-assisted multicore microstructured optical fiber, Sens. Actuators B Chem. 365 (2022) 131941.

[108] L. Nguyen, K. Hill, S. Warren-Smith and T. Monro, Interferometric-type optical biosensor based on exposed core microstructured optical fiber, Sens. Actuators B Chem. 221 (2015) 320–327.

[109] F. Li, X. Li, X. Zhou, P. Gong, Y. Zhang, Y. Zhao and L. Nguyen, H. Ebendorff-Heidepriem and S. Warren-Smith, Plug-in label-free optical fiber DNA hybridization sensor based on C-type fiber Vernier effect, Sens. Actuators B Chem. 354 (2022) 131212.

[110] L. Chen, Y. Leng, B. Liu, J. Liu, S. Wan, T. Wu, J. Yuan, L. Shao, G. Gu, Y. Fu, H. Xu, Y. Xiong, X. He and Q. Wu, Ultrahigh-sensitivity label-free optical fiber biosensor based on a tapered singlemode-no core-singlemode coupler for Staphylococcus aureus detection, Sens. Actuators B Chem., 320 (2020) 128283.

[111] R. Kumar, Y. Leng, B. Liu, J. Zhou, L. Shao, J. Yuan, X. Fan, S. Wan, T. Wu, J. Liu, R. Binns, Y. Fu, W. Ng, G. Farrell, Y. Semenova, H. Xu, Y. Xiong, X. He and Qiang Wu, Ultrasensitive biosensor based on magnetic microspheres enhanced microfiber interferometer, Biosens. Bioelectron. 145 (2019) 111563.

[112] X. Li, L. Nguyen, Y. Zhao, H. Ebendorff-Heidepriem and S. Warren-Smith, High-sensitivity Sagnac-interferometer biosensor based on exposed core microstructured optical fiber, Sens. Actuators B Chem. 269 (2018) 103–109.

[113] X. Li, N. Chen, X. Zhou, Y. Zhang, Y. Zhao, L. Nguyen, H. Ebendorff-Heidepriem and S. Warren-Smith, In-situ DNA detection with an interferometric-type optical sensor based on tapered exposed core microstructured optical fiber, Sens. Actuators B Chem. 351 (2022) 130942.

[114] N. Zhang, K. Li, Y. Cui Z. Wu, P. Shum, J. Auguste, X. Dinh, G. Humbert and L. Wei, Ultra-sensitive chemical and biological analysis via specialty fibers with built-in microstructured optofluidic channels, Lab Chip, 18 (2018) 655.

[115] B. Schyrr, S. Paschec, E. Scolana, R. Ischer , D. Ferrarioa, J. Porchet and G. Voirin, Development of a polymer optical fiber pH sensor for on-body monitoring application, Sens. Actuators B Chem. 194 (2014) 238–248.

[116] B. Quandt, F. Braun, D. Ferrario, R. Rossi, A. Scheel-Sailer, M. Wolf, G. Bona, R. Hufenus, L. Scherer and L. Boesel, Body-monitoring with photonic textiles: a reflective heartbeat sensor based on polymer optical fibres, J. R. Soc. Interface 14 (2017) 0060.

[117] Y. Wang, B. Liu, Y. Pang, J. Liu, J. Shi, S. Wan, X. He, J. Yuan and Q. Wu, Low-cost wearable sensor based on a D-shaped plastic optical fiber for respiration monitoring, IEEE T Instrum Meas. 70 (2021) 1-8.

[118] A. Leal-Junior, L. Avellar, V. Biazi, M. Soares, A. Frizera and C. Marques. Multifunctional flexible optical waveguide sensor: on the bioinspiration for ultrasensitive sensors development. Opto-Electron Adv 5 (2022) 210098.

[119] A. Leal-Junior, C. Marques, A. Frizera and M. J. Pontes, Dynamic Mechanical Analysis on a PolyMethyl Methacrylate (PMMA) Polymer Optical Fiber, IEEE Sens. J. 18 (6) (2018) 2353-2361.

[120] T. Saini and R. Sinha, Mid-infrared supercontinuum generation in soft-glass specialty optical fibers: A review, Prog. Quantum. Electron 78 (2021) 100342.

[121] B. Li, M. Wu, X. Liu, G. Zhou, J. Liu. Z. Hou, and C. Xia, Surface plasmon resonance on the V-type microstructured optical fiber embedded with dual copper wires, Plasmonics, 14 (2019) 383–387.

[122] H. Lee, M. Schmidt, R. Russell, N. Joly, H. Tyagi, P. Uebel, and P. Russell, Pressure-assisted melt-filling and optical characterization of Au nano-wires in microstructured fibers, Opt. Express 19 (13) (2014) 12180-12189.

[123] I. Donald, Production, properties and applications of microwire and related products, J. Mater. Sci. 22, (1987) 2661-2679.

[124] V. S. Chaudhary, D. Kumar and S. Kumar, SPR-Assisted Photonic Crystal Fiber-Based Dual-Wavelength Single Polarizing Filter With Improved Performance, IEEE T. Plasma Sci. 49 (12) (2021) 3803-3810.

[125] Y. Zhao, S. Li, Q. Liu and X. Wang, Design of a novel photonic crystal fiber filter based on gold-coated and elliptical air holes, Optical Materials, 73 (2017) 638-641.

[126] W. Yan, A. Page, T. Nguyen-Dang, Y. Qu, F. Sordo, L. Wei, and F. Sorin, Advanced Multimaterial Electronic and Optoelectronic Fibers and Textiles, Adv. Mater. 31 (2019) 1802348.

[127] A. Canales, X. Jia, U. Froriep, R. Koppes, C. Tringides, J. Selvidge, C. Lu, C. Hou, L. Wei, Y. Fink and P. Anikeeva, Multifunctional fibers for simultaneous optical, electrical and chemical interrogation of neural circuits in vivo, Nat. Biotechnol 33 (3) (2015) 277-284.

[128] S. Jiang, D. Patel, J, Kim, S. Yang, W. Mills, Y. Zhang, K. Wang, Z. Feng, S. Vijayan, W. Cai, A. Wang, Y. Guo, I. Kimbrough, H. Sontheimer and X. Jia, Spatially expandable fiber-based probes as a multifunctional deep brain interface, Nat. Commun. 11 (2020) 6115.

[129] J. Wang, Z. Liu, S. Gao, A. Zhang, Y. Shen, and H. Tam, Fiber-Optic Anemometer Based on Bragg Grating Inscribed in Metal-Filled Microstructured Optical Fiber, IEEE J. Lightwave Technol. 34 (21) (2016) 4884-4889.

[130] G. Woyessa, K. Nielsen, A. Stefani, C. Markos, and O. Bang, Temperature insensitive hysteresis free highly sensitive polymer optical fiber Bragg grating humidity sensor, Opt. Express 24 (2) (2016) 1206-1213.

[131] K. Chen, X. Zhou., X. Cheng, R. Qiao, Y. Cheng, C. Liu, Y. Xie, W. Yu, F. Yao, Z. Sun, F. Wang, K. Liu and Z. Liu. Graphene photonic crystal fibre with strong and tunable light–matter interaction, Nat. Photonics 13 (2019) 754–759.

[132] R. M. Silva, M. S. Ferreira, J. Kobelke, K. Schuster, and O. Frazão, Simultaneous measurement of curvature and strain using a suspended multicore fiber, Opt. Lett. 36 (2011) 3939-3941.

[133] L. Htein, D. Gunawardena, Z. Liu, and H. Tam, Two semicircular-hole fiber in a Sagnac loop for simultaneous discrimination of torsion, strain and temperature, Opt. Express 28 (23) (2020) 33841-33853.

[134] Y. Li, L. Wang, Y. Chen, D. Yi, F. Teng, X. Hong, X. Li, Y. Geng, Y. Shi, and D. Luo, High-performance fiber sensor via Mach-Zehnder interferometer based on immersing exposed-core microstructure fiber in oriented liquid crystals, Opt. Express 28 (3) (2020) 3576-3586.

[135] M. Azkune, T. Frosch, E. Arrospide, G. Aldabaldetreku, I. Bikandi, J. Zubia, J.Popp, and T. Frosch, Liquid-core microstructured polymer optical fiber as fiber-enhanced raman spectroscopy probe for glucose sensing, IEEE J. Lightwave Technol. 37 (13) (2019) 2981-2988.

[136] Y. Tian, G. Xiao, Y. Luo, J. Zhang, L. Yuan, Microhole fiber-optic sensors for nanoliter liquid measurement, Opt. Fiber Technol. 72 (2022) 102981.

[137] M. I. Reja, L. V. Nguyen, L. Peng, H. Ebendorff-Heidepriem and S. Warren-Smith, Temperature-Compensated Interferometric High-Temperature Pressure Sensor Using a Pure Silica Microstructured Optical Fiber, IEEE T. Instrum. Meas. 71 (2022) 1-12.

[138] V. Chaudhary, D. Kumar, G. P. Mishra, S. Sharma and S. Kumar, Plasmonic biosensor with gold and titanium dioxide immobilized on photonic crystal fiber for blood composition detection, IEEE Sens. J. 22 (9) (2022) 8474-8481.

[139] V. Chaudhary, D. Kumar and S. Kumar, Gold-immobilized photonic crystal fiber-based SPR biosensor for detection of malaria disease in human body, IEEE Sens. J. 21 (16) (2021) 17800-17807.

[140] R. Srivastava, Y. Prajapati, S. Pal and S. Kumar, Micro-channel plasmon sensor based on a D-shaped photonic crystal fiber for malaria diagnosis with improved performance, IEEE Sens. J. 22 (15) (2022) 14834-14841.

[141] Y. Wang, G. Zhu, M. Li, R. Singh, C. Marques, R. Min, B. Kaushik, B. Zhang, R. Jha, and S. Kumar, Water Pollutants p-Cresol Detection Based on Au-ZnO Nanoparticles Modified Tapered Optical Fiber, IEEE T. Nanobiosci 20 (3) (2021) 377-384.

[142] X. Liu, R. Singh, M. Li, G. Li, R. Min, C. Marques, B. Zhang and S. Kumar, Plasmonic sensor based on offset-splicing and waist-expanded taper using multicore fiber for detection of Aflatoxins B1 in critical sectors, Opt. Express 31 (2023) 4783-4802.

[143] M. Li, R. Singh, C. Marques, B. Zhang, and S. Kumar, 2D material assisted SMF-MCF-MMF-SMF based LSPR sensor for creatinine detection, Opt. Express 29 (2021) 38150-38167.

[144] M. Li, R. Singh, M. Soares, C. Marques, B. Zhang, and S. Kumar, Convex fiber-tapered seven core fiber-convex fiber (CTC) structure-based biosensor for creatinine detection in aquaculture, Opt. Express 30 (2022) 13898-13914.

[145] Z. Wang, R. Singh, C. Marques, R. Jha, B. Zhang, and S. Kumar, Taper-in-taper fiber structure-based LSPR sensor for alanine aminotransferase detection, Opt. Express 29 (2021) 43793-43810.

[146] S.Jain, K. Choudhary, S. Kumar, Photonic crystal fiber-based SPR sensor for broad range of refractive index sensing applications, Opt. Fiber Technol 73 (2022) 103030.

[147] A. Leal-Junior, J. Guo, R. Min, A. Fernandes, A. Frizera and C. Marques, Photonic smart bandage for wound healing assessment Photon. Res. 9 (2021) 272-280.

[148] M. Soares, M. Vidal, N. Santos, F. Costa, C. Marques, S. Pereira, and C. Leitão, Immunosensing based on optical fiber technology: recent advances, Biosensors. 11 (9) (2021) 305.

[149] M. Li, R. Singh, Y. Wang, C. Marques, B. Zhang and S. Kumar, Advances in Novel Nanomaterial-Based Optical Fiber Biosensors—A Review, Biosensors. 12 (10) (2022) 843.

[150] A. Leal-Junior, V. Campos, C. Díaz, R. Andrade, A. Frizera, and C. Marques, A machine learning approach for simultaneous measurement of magnetic field position and intensity with fiber Bragg grating and magnetorheological fluid, Opt. Fiber Technol. 56 (2020) 102184.